Mitophagy-dependent necroptosis contributes to the pathogenesis of COPD

Kenji Mizumura,[1,2,3] Suzanne M. Cloonan,[1,2] Kiichi Nakahira,[1,2] Abhiram R. Bhashyam,[2] Morgan Cervo,[4] Tohru Kitada,[5] Kimberly Glass,[6] Caroline A. Owen,[2] Ashfaq Mahmood,[4] George R. Washko,[2] Shu Hashimoto,[3] Stefan W. Ryter,[1,2] and Augustine M.K. Choi[1,2]

[1]Joan and Sanford I. Weill Department of Medicine, New York-Presbyterian Hospital, Weill Cornell Medical College, New York, New York, USA. [2]Division of Pulmonary and Critical Care Medicine, Brigham and Women's Hospital, Harvard Medical School, Boston, Massachusetts, USA. [3]Division of Respiratory Medicine, Nihon University School of Medicine, Tokyo, Japan. [4]Department of Radiology, Brigham and Women's Hospital, Harvard Medical School, Boston, Massachusetts, USA. [5]Division of Neuroscience, Ottawa Hospital Research Institute, Ottawa, Ontario, Canada. [6]Department of Biostatistics and Computational Biology, Dana-Farber Cancer Institute and Harvard School of Public Health, Boston, Massachusetts, USA.

The pathogenesis of chronic obstructive pulmonary disease (COPD) remains unclear, but involves loss of alveolar surface area (emphysema) and airway inflammation (bronchitis) as the consequence of cigarette smoke (CS) exposure. Previously, we demonstrated that autophagy proteins promote lung epithelial cell death, airway dysfunction, and emphysema in response to CS; however, the underlying mechanisms have yet to be elucidated. Here, using cultured pulmonary epithelial cells and murine models, we demonstrated that CS causes mitochondrial dysfunction that is associated with a reduction of mitochondrial membrane potential. CS induced mitophagy, the autophagy-dependent elimination of mitochondria, through stabilization of the mitophagy regulator PINK1. CS caused cell death, which was reduced by administration of necrosis or necroptosis inhibitors. Genetic deficiency of PINK1 and the mitochondrial division/mitophagy inhibitor Mdivi-1 protected against CS-induced cell death and mitochondrial dysfunction in vitro and reduced the phosphorylation of MLKL, a substrate for RIP3 in the necroptosis pathway. Moreover, *Pink1*$^{-/-}$ mice were protected against mitochondrial dysfunction, airspace enlargement, and mucociliary clearance (MCC) disruption during CS exposure. Mdivi-1 treatment also ameliorated CS-induced MCC disruption in CS-exposed mice. In human COPD, lung epithelial cells displayed increased expression of PINK1 and RIP3. These findings implicate mitophagy-dependent necroptosis in lung emphysematous changes in response to CS exposure, suggesting that this pathway is a therapeutic target for COPD.

Introduction

Chronic obstructive pulmonary disease (COPD) contributes significantly to the global burden of disease as the fourth leading cause of mortality worldwide (1). This disease includes clinical phenotypes of emphysema (loss of alveolar surface area) and bronchitis associated with mucus obstruction of the airways (2). The pathogenesis of COPD remains incompletely understood but may involve aberrant inflammatory and cellular responses (e.g., apoptosis) in the lung in response to cigarette smoke (CS), the major risk factor for this disease (3, 4).

Using cellular and animal models of CS exposure as well as human lung tissue from patients with COPD, we have previously demonstrated a role for the cellular macroautophagic pathway (hereafter abbreviated as autophagy) in the pathogenesis of COPD (5, 6). Autophagy is a homeostatic program in which cytosolic proteins or organelles are assimilated into double-membrane autophagosomes and subsequently transferred to the lysosomes for degradation (7). Lung tissue derived from COPD patients or from mice chronically exposed to CS displayed increased autophagosome numbers and increased expression of autophagy proteins (5, 6). Genetic deletion of crucial autophagy proteins (e.g., beclin 1 and microtubule-associated protein-1 light chain-3B [LC3B]) ameliorated CS-induced lung epithelial cell death in response to CS exposure (5, 6). LC3B-null mice (*Map1lc3B*$^{-/-}$) were resistant to CS-induced airspace enlargement during chronic CS exposure (6). Furthermore, *Map1lc3B*$^{-/-}$ or *Becn1*$^{+/-}$ mice were resistant to mucociliary clearance (MCC) disruption in the airways after subchronic CS exposure in vivo (8). To date, the specific mechanisms by which autophagy can promote COPD pathogenesis remain incompletely understood.

In addition to autophagy, highly selective pathways for autophagic processing of subcellular components involve ubiquitination and recruitment of cargo adaptor proteins such as p62^{SQSTM1} (9, 10). One such pathway, mitophagy, targets mitochondria for autophagic degradation (11). Genetic deletion of the genes encoding PTEN-induced kinase 1 (*PINK1*) and Parkin (*PARK2*) causes progressive mitochondrial damage associated with Parkinson's disease (12, 13). In neurons, depolarized mitochondria stabilize PINK1, which subsequently recruits Parkin, an E3 ubiquitin ligase that ubiquitinylates mitochondrial outer membrane proteins (11). Increasing evidence suggests that mitophagy is relevant to human diseases (11, 14). However, the specific role of mitophagy in lung diseases, in particular COPD, has previously not been described.

Conflict of interest: The authors have declared that no conflict of interest exists.
Submitted: January 2, 2014; **Accepted:** June 6, 2014.
Reference information: *J Clin Invest*. 2014;124(9):3987–4003. doi:10.1172/JCI74985.

Mitophagy is considered a homeostatic program that maintains a healthy mitochondrial population and plays largely cytoprotective roles in the context of disease pathogenesis (11). In contrast, an emerging view also implicates mitophagy as a possible effector of cell death programs. Specifically, ceramide-initiated cell death required mitophagy, involving LC3-ceramide interactions at the mitochondria (15). These observations, along with our previous studies implicating autophagy as a propathogenic mediator in COPD, led us to the hypothesis that mitophagy is associated with epithelial cell death in COPD.

Exposure to CS has been reported to cause cell death by apoptosis and necrosis (16). While apoptosis denotes a genetically programmed pathway involving caspase activation, necrosis is characterized as cell death induced by extreme physical or chemical stress (17). However, recent studies suggest the existence of a genetically programmed and regulated form of necrosis, termed necroptosis (18). The receptor-interacting protein-1 and -3 (RIP1/3) kinases, which form a multiprotein complex termed the necrosome, are key regulators of necroptosis (18–20). Although activation of the necrosome may involve a decline in mitochondrial integrity and impaired energy metabolism, the precise mechanisms remain unclear (18). Recent studies suggest a relevance of RIP3-dependent necroptosis to human diseases (21–23). To date, the role of necroptosis in COPD pathogenesis has not been studied.

In the current study, we show that CS induced mitophagy and mitochondrial dysfunction in epithelial cells. We demonstrate that mitophagy was associated with epithelial cell death, specifically involving necroptosis, in response to CS exposure. We show that genetic deletion of PINK1, a key mitophagy regulator, and treatment with the mitochondrial division/mitophagy inhibitor Mdivi-1 reduced CS-dependent activation of necroptosis in vitro. Using in vivo models of COPD pathogenesis, we demonstrate the importance of mitophagy in the development of experimental emphysema and airway disruption. Furthermore, we demonstrate the elevated expression of PINK1 and RIP3 in human COPD lung. Taken together, these findings suggest that mitophagy-dependent necroptosis plays a pathogenic role in COPD and may represent a new therapeutic target in this disease.

Results

Cigarette smoke extract can induce mitochondrial dysfunction in pulmonary epithelial cells. To study the effect of CS on mitochondrial integrity, we treated primary human bronchial epithelial (HBE) cells (Beas-2B) with aqueous cigarette smoke extract (CSE), an in vitro model of CS exposure. Treatment of Beas-2B cells with CSE increased the abundance of swollen mitochondria, with evidence of severely disrupted cristae, as detected by electron microscopy (Figure 1A). Furthermore, oxygen consumption rate (OCR) analysis in vitro revealed that CSE exposure dose-dependently reduced basal mitochondrial respiration in Beas-2B cells (Figure 1B).

Next, we evaluated the functional mitochondrial pool in Beas-2B cells exposed to CSE using tetramethylrhodamine ethyl ester (TMRE), a fluorescent probe sensitive to mitochondrial membrane potential. The functional mitochondrial pool was assessed after 4 hours of CSE exposure, during which epithelial cells remained viable (Supplemental Figure 1A; supplemental material available online with this article; doi:10.1172/JCI74985DS1). CSE treatment caused a marked decrease in functional mitochondria in Beas-2B cells (Figure 1C) and primary human bronchial epithelial (HBE) cells (Supplemental Figure 1B). The significant mitochondrial depolarization that occurred in Beas-2B cells in response to CSE, as detected by TMRE, could be inhibited by cyclosporine A (CsA), an inhibitor of mitochondrial membrane permeability transition (Supplemental Figure 1C). We observed that CSE treatment increased mitochondrial reactive oxygen species (mtROS) production in Beas-2B cells (Figure 1D) and HBE cells (Supplemental Figure 1D), as detected by MitoSOX, a fluorescent indicator of mitochondrial superoxide anion radical (O_2^-) production. In Beas-2B cells, we found that mtROS production increased within 30 minutes of treatment and remained stable for 2 hours. The mtROS production further increased in a time-dependent manner up to 24 hours after treatment (Figure 1D). These data, taken together, implicate mitochondrial dysfunction in the adverse effects of CSE in vitro.

CSE can regulate PINK1, but not Parkin, in pulmonary epithelial cells. Mitophagy is a cellular response commonly associated with mitochondrial dysfunction (11). PINK1 and Parkin represent well-characterized regulators of mitophagy in neural cells and tissues (13). Given that CSE could induce mitochondrial dysfunction in epithelial cells, we investigated the expression of PINK1 under these conditions. Comparative quantitative PCR (qPCR) analysis indicated that *PINK1* mRNA is expressed in human lung tissue, albeit at a lower relative abundance than in brain tissue (Supplemental Figure 2A). Exposure to CSE increased the relative abundance of PINK1 in Beas-2B, with a maximum detected at 8 hours (Figure 2, A and C). We observed similar results in HBE cells (Supplemental Figure 2B). Similar to the results with *PINK1* mRNA, we detected *PARK2* mRNA in human trachea and lung tissue (Supplemental Figure 2C). Comparative qPCR analysis indicated that there was little expression of *PARK2* mRNA in HBE cells and Beas-2B cells (Supplemental Figure 2D). Western immunoblot analysis showed no Parkin protein in Beas-2B cells relative to that detected in positive controls from human neural cells and mouse brain tissue, and its expression did not increase with exposure to CSE (Supplemental Figure 2E).

CSE-induced mtROS can regulate the phosphorylation (Ser616) of the fission regulator dynamin-related protein 1 and the mitophagy regulator PINK1 in pulmonary epithelial cells. Mitochondrial dynamics play a key role in the response of cells to exogenous stress. Mitochondrial fission is necessary to trigger mitophagy (24). Dynamin-related protein 1 (Drp1) is a known regulator of mitochondrial fission. The phosphorylation of Drp1 on Ser616 promotes Drp1 recruitment to mitochondria and subsequent fission (25). Therefore, we tested whether CSE can regulate Drp1 in Beas-2B cells. We found that CSE induced phosphorylation of Drp1 at Ser616 (Figure 2, B and C). Confocal image analysis detected Tom20 staining, indicating that CSE exposure promoted the colocalization of Ser616 phosphorylated Drp1 (p-Drp1) with mitochondria, which signifies the initiation of the fission pathway (Figure 2D).

To verify the role of mtROS in PINK1 expression and the phosphorylation of Drp1 (Ser616) in response to CSE, we used mitoquinone (MitoQ), a mitochondria-targeted antioxidant.

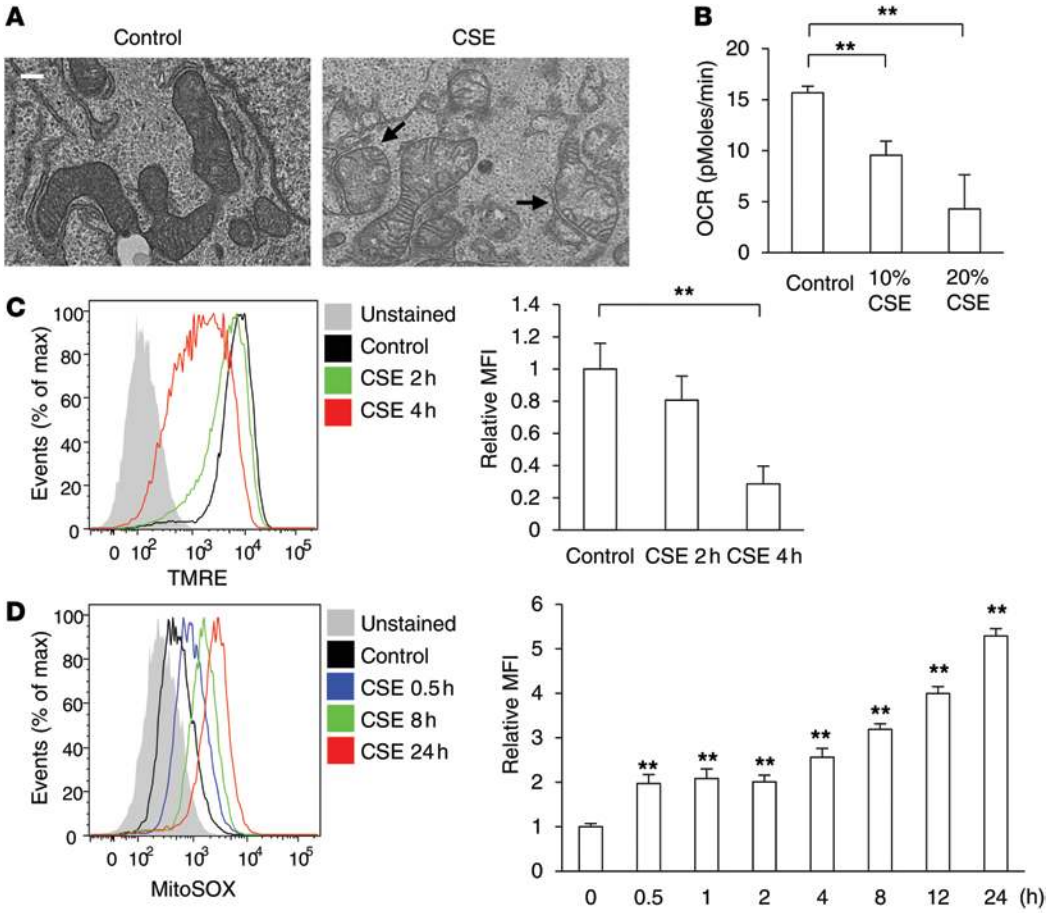

Figure 1. CSE causes mitochondrial dysfunction in pulmonary epithelial cells. (**A**) Representative TEM images (original magnification, ×10,000) of morphological changes in mitochondria (black arrows) in Beas-2B cells that were either left untreated or treated with 20% CSE for 4 hours. Scale bar: 400 nm. Image is representative of 10 images/sample; *n* = 2 samples/condition. (**B**) Beas-2B cells were left untreated or treated with the indicated percentage of CSE for 4 hours. OCR in Beas-2B cells was measured using a Seahorse XF96 analyzer. *n* = 6 samples/condition. (**C**) Flow cytometry of Beas-2B cells left unstained or labeled with TMRE, followed by treatment with 20% CSE for the indicated times. Data are representative of 3 experiments. (**D**) Flow cytometry of CSE-treated Beas-2B cells left unstained or labeled with MitoSOX following treatment with 20% CSE for the indicated times. Data are representative of 3 experiments. The *x* axis shows the fluorescent signal intensity, and the *y* axis represents the cell number normalized as a percentage of the maximum (% of max) (**C** and **D**). All data represent the mean ± SEM (**B**–**D**). $^{**}P < 0.01$ by unpaired, 2-tailed Student's *t* test (**B**–**D**) versus control (**D**).

Treatment of Beas-2B cells with MitoQ effectively inhibited the detection of mtROS in Beas-2B cells (Figure 2E). Treatment with MitoQ significantly inhibited the stabilization of PINK1 induced by CSE treatment relative to that observed in vehicle control (Figure 2F). Furthermore, treatment with MitoQ significantly inhibited the phosphorylation of Drp1 induced by CSE treatment relative to that in vehicle control (Figure 2G). Taken together, these experiments suggest that both PINK1 stabilization and phosphorylation of Drp1 are events that can be inhibited by scavengers of mtROS.

CSE can induce PINK1-dependent mitophagy in pulmonary epithelial cells. Given that CSE could induce PINK1 expression and phosphorylation of Drp1 through mtROS production in epithelial cells, we next investigated the occurrence of mitophagy and mitochondrial fission under these conditions. Beas-2B cells in response to CSE treatment showed similar morphological changes in mitochondria undergoing mitophagy, as previously described (26), including partial mitochondrial clearance with perinuclear compaction of mitochondria and mitochondrial fission (Figure 3A). We quantified mitochondrial fission in the cytoplasm outside of the perinuclear compaction area (see Methods). Consistent with the kinetics of Drp1 phosphorylation, the percentage of cells exhibiting mitochondrial fission began to increase after 1 hour of CSE treatment (20%) and continued to increase during the first 4 hours (Figure 2, B and C, and Figure 3A). Consistent with the kinetics of PINK1 expression, Beas-2B cells displayed significant mitochondrial clearance after 4 hours of CSE treatment (Figure 2, A and C, and Figure 3A). After 8 hours, mitochondria in the cytosol outside of the perinuclear compaction area disappeared almost completely (Figure 3A). Due to the incidence of mitochondrial clearance, we did not detect cytosolic mitochondrial fission events after 8 hours. In contrast, we observed perinuclear mitochondrial compaction as early as 2 hours after CSE treatment, which continued to increase to a plateau at 24 hours (Figure 3A).

We next used the mitochondria-targeted mKeima (mt-mKeima) probe to detect functional mitophagy (27). Since mt-mKeima is resistant to lysosomal proteases and exhibits a reversible change in color in response to acidic pH, mt-mKeima can be used to monitor autolysosome maturation. A high excitation peak ratio (550_{ex}:438_{ex}) of mt-mKeima, represented by a pseudo-red color, indicates the presence of mitochondria in maturing autolysosomes. Using this assay, we found that the incidence of red mt-mKeima puncta, indicative of mitophagy, significantly increased in cultured Beas-2B cells exposed to CSE relative to that observed in the untreated cells (Figure 3B).

After CSE exposure, PINK1 expression preferentially increased in the mitochondrial fraction of Beas-2B cells (Figure 3C). In parallel with increases in the abundance of mitochondrial PINK1, we found that marked increases in the abundance of ubiquitin, which determines selectivity in mitophagy (9, 11), occurred in the mitochondrial fraction of CSE-treated Beas-2B cells (Figure 3C).

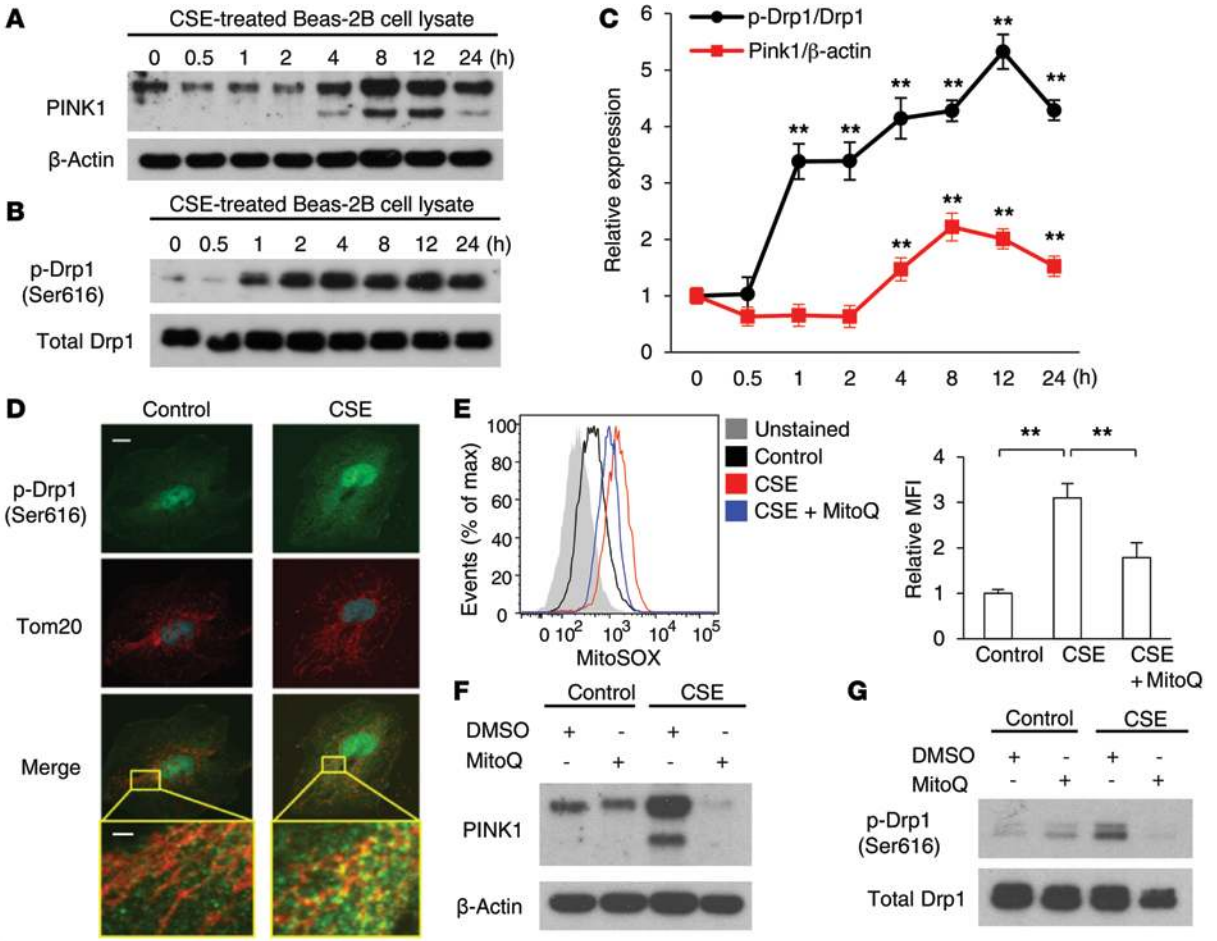

Figure 2. CSE induces PINK1 expression and phosphorylation of Drp1 (Ser616), which is regulated by mitochondrial ROS. Immunoblot analysis of PINK1 (**A**) and p-Drp1 (**B**) in cell lysates from Beas-2B cells treated with 20% CSE at the indicated times. β-Actin and total Drp1 served as the standards. (**C**) p-Drp1 and PINK1 expression was assessed by densitometry of immunoblots. Band intensities were normalized to total Drp1 and β-actin. Data are representative of 3 experiments. (**D**) Immunofluorescence staining for p-Drp1 (green), Tom20 (red), and nuclei (blue) in Beas-2B cells treated with 20% CSE for 1 hour. Scale bar: 10 μm. Areas outlined in yellow are shown enlarged in the bottom panels (scale bar: 2 μm). Image (original magnification, ×120) is representative of 5 images/slide; $n = 3$ slides/condition. (**E**) Flow cytometry of Beas-2B cells labeled with MitoSOX. Beas-2B cells were incubated for 1 hour with MitoQ (10 μM) or vehicle (DMSO) and treated with 20% CSE for 4 hours. The *x* axis shows the fluorescent signal intensity, and the *y* axis represents the cell number normalized as a percentage of the maximum (% of max). Data are representative of 3 experiments. Immunoblot analysis of PINK1 (**F**) and p-Drp1 (**G**). Beas-2B cells were incubated for 1 hour with MitoQ (50 μM) or vehicle (DMSO) and treated with 20% CSE for 8 hours. β-Actin and total Drp1 served as the standards. All data represent the mean ± SEM (**C** and **E**). $^{**}P < 0.01$ by unpaired, 2-tailed Student's *t* test (**C** and **E**) versus control (**C**).

To verify the role of PINK1 in CSE-induced mitophagy, we isolated pulmonary epithelial cells from *Pink1*$^{-/-}$ mice and their corresponding *Pink1*$^{+/+}$ wild-type littermates. *Pink1*$^{-/-}$ cells exhibited no mitochondrial clearance or perinuclear compaction in response to CSE relative to wild-type cells (Figure 3D). These results, taken together, suggest that functional PINK1-dependent mitophagy occurs as a result of CSE exposure.

Inhibition of mitochondrial fission and mitophagy restores CSE-induced mitochondrial depolarization. We used Mdivi-1, a known inhibitor of mitochondrial fission, as a tool to study the relationships between mitophagy and mitochondrial dysfunction. Although Mdivi-1 is characterized as a pharmacological inhibitor of Drp1, recent studies have also implicated Mdivi-1 as an inhibitor of mitophagy (28–31). We first tested the efficacy of this compound as an inhibitor of mitochondrial fission in response to CSE. We observed that the percentage of cells exhibiting mitochondrial fission continued to increase in the first 4 hours (Figure 3A and Figure 4A). Treatment with Mdivi-1 significantly reduced mitochondrial fission events relative to those observed in vehicle-treated cells (Figure 4A).

Next, we tested the efficacy of this compound as an inhibitor of mitophagy using the mt-mKeima assay, an indicator of mitochondrial colocalization with maturing autolysosomes. We found that treatment with Mdivi-1 reduced the incidence of red puncta, indicative of mitophagy, in mt-mKeima–transfected Beas-2B cells exposed to CSE relative to CSE-exposed cells treated with vehicle alone (Figure 4B). Consistent with this apparent inhibitory effect on mitophagy, Mdivi-1 inhibited the increase in mitochondrial ubiquitination observed after CSE treatment (Figure 4C). To further investigate the relationship between mitophagy and mitochondrial depolarization, we treated Beas-2B cells with CSE in the absence and presence of Mdivi-1 and measured mitochondrial

integrity using TMRE. Interestingly, we found that treatment with Mdivi-1 restored a CSE-induced decline of $\Delta\Psi_m$ (Figure 4D). These results suggest that chemical inhibition of mitophagy results in the preservation of mitochondrial function in the CSE toxicity model.

PINK1-dependent mitophagy affects mitochondrial membrane potential and cell death during CSE exposure. Experiments with mitochondrial uncoupling agents have suggested that mitochondrial depolarization is a potential initiating event in mitophagy that triggers stabilization of PINK1 (11). However, the effects of PINK1 on mitochondrial depolarization are not well understood. To investigate the relationship between PINK1 and mitochondrial depolarization during CSE-induced stress, we isolated pulmonary epithelial cells from *Pink1*$^{-/-}$ mice and their corresponding *Pink1*$^{+/+}$ wild-type littermates and subjected them to CSE. Surprisingly, *Pink1*$^{-/-}$ cells were resistant to CSE-induced mitochondrial depolarization, as indicated by TMRE (Figure 5A). These results suggest that the mitophagy protein PINK1 contributes to mitochondrial depolarization during CSE exposure.

Since PINK1 expression is regulated by mtROS (Figure 2F) generated by CSE exposure, we also tested the potential for exogenous ROS to modulate these responses using the model oxidant compound H_2O_2. Although treatment of Beas-2B cells with H_2O_2 (500 μM) caused mitochondrial depolarization, as detected by TMRE, we observed no significant difference in the response between *Pink1*$^{+/+}$ and *Pink1*$^{-/-}$ cells (Supplemental Figure 1E). This is in contrast to our findings that CSE exposure, which stimulates endogenous mtROS, caused mitochondrial depolarization in wild-type cells, which was significantly reduced in *Pink1*$^{-/-}$ epithelial cells, highlighting the selectivity of the mitochondrial response.

The relationships between autophagy, its selective subtype mitophagy, and cellular death programs remain incompletely understood (32). To examine the relationship between mitochondrial depolarization and cell death, we treated Beas-2B cells with CsA, an inhibitor of mitochondrial membrane permeability transition. Beas-2B cells treated with CsA, which were resistant to loss of $\Delta\Psi_m$ induced by CSE (Supplemental Figure 1C), were also resistant to CSE-induced cell death (Figure 5B).

To examine the role of PINK1-dependent mitophagy in CSE-induced epithelial cell death in vitro, we isolated pulmonary alveolar epithelial cells from *Pink1*$^{-/-}$ mice and their corresponding *Pink1*$^{+/+}$ wild-type littermates. Alveolar epithelial cells were subjected to CSE treatment, followed by assessment of cytotoxicity, as determined by LDH release. *Pink1*$^{-/-}$ cells were resistant to CS-induced cytotoxicity relative to *Pink1*$^{+/+}$ cells (Figure 5C). These results suggest that PINK1 promotes cell death in response to CSE. Similarly, treatment with Mdivi-1 reduced CSE-induced cell death in Beas-2B cells (Figure 5D), which suggests that mitophagy plays a role in this process.

Mitophagy regulates cell death involving necroptosis through PINK1 and mitochondria-dependent pathways. Previously, autophagy-associated cell death, as observed during caspase inhibition, has been suggested to involve necroptosis (33). It is not known whether mitophagy can regulate necroptosis. We therefore assessed the role of necrosis and necroptosis in CSE-induced cell death and their relationship to mitophagy. CSE-induced cell death was effectively reduced by treatment with necrox-5 (Nex-5), a necrosis inhibitor with antioxidant activity that localizes primarily in the mitochondria, or with necrostatin-1 (Nec-1), a necroptosis inhibitor, in Beas-2B cells (Figure 6A). Furthermore, CSE treatment increased chromatin protein high-mobility group B1 (HMGB1), a biomarker of necrosis, in the supernatant of Beas-2B cells (Supplemental Figure 3A).

The mixed-lineage kinase domain–like (MLKL) protein is phosphorylated by RIP3 at Thr357 and Ser358 residues, and these events are critical for execution of necroptosis (34). We therefore first examined MLKL Thr357 phosphorylation in CSE-treated Beas-2B cells (Figure 6B) and HBE cells (Supplemental Figure 3B). CSE treatment resulted in increased MLKL phosphorylation in Beas-2B cells and HBE cells, consistent with activation of the necrosome. Furthermore, we examined the effect of genetic depletion of PINK1 on CSE-induced MLKL phosphorylation using *PINK1*-targeted siRNA (Figure 6C). CSE-induced MLKL phosphorylation was decreased in *PINK1*-knockdown cells. Similarly, we observed that Mdivi-1 treatment inhibited MLKL phosphorylation induced by CSE in Beas-2B cells (Figure 6D). In contrast, the chemical inhibitors Nec-1 and Nex-5 had no effect on CSE-induced PINK1 expression (Supplemental Figure 3C).

Finally, to examine the relationship between mitophagy and necroptosis, we analyzed PINK1, ubiquitin, RIP1, RIP3, and MLKL expression in mitochondrial and cytosolic fractions isolated from Beas-2B cells exposed to CSE (Figure 6E). PINK1, ubiquitin, RIP1, RIP3, and MLKL colocalized with the mitochondria of Beas-2B cells after CSE treatment. MLKL phosphorylation increased in the mitochondrial fraction of CSE-treated cells relative to that in untreated cells. Interestingly, treatment with CsA reduced MLKL phosphorylation, while it had no effect on CSE-induced PINK1 or ubiquitin accumulation (Figure 6E). These results suggest that mitochondrial depolarization occurs upstream of necrosome activation in pulmonary epithelial cells treated with CSE.

CS induces autophagic turnover of mitochondria and PINK1-dependent mitochondrial dysfunction in vivo. Next, we sought to determine the relevance of our in vitro observations of mitophagy and mitochondrial dysfunction to in vivo models of CS exposure. To assess the processing of mitochondrial components by the autophagosome/lysosome pathway, we used a novel tissue fractionation assay for autophagosomes (8). LC3B-GFP mice were exposed to CS for 3 weeks, with corresponding room air (RA) controls, and then autophagosome/lysosome-enriched (LE-enriched) fractions were isolated from lung tissue and immunoprecipitated with anti-GFP. We found that exposure of mice to CS resulted in dramatic increases in the accumulation of mitochondrial components (i.e., complex III, complex V, and Hsp60) in LC3B-immunoprecipitated LE fractions obtained from lung tissue, suggestive of increased processing of these components by autophagy (Figure 7, A–C).

To examine the functional role of mitophagy in mitochondrial integrity in vivo, we performed the JC-1 assay to evaluate $\Delta\Psi_m$ in the lungs of *Pink1*$^{-/-}$ or *Pink1*$^{+/+}$ mice subjected to CS exposure for 6 months (Figure 7D). *Pink1*$^{+/+}$ mice exposed to CS displayed a marked reduction of $\Delta\Psi_m$. In contrast, *Pink1*$^{-/-}$ mice exposed to CS maintained mitochondrial integrity in the lungs relative to that observed in *Pink1*$^{+/+}$ mice (Figure 7D). Taken together, these experiments suggest that mitophagy occurs in vivo in response to CS and that, consistent with in vitro observations, PINK1 contributes to mitochondrial depolarization in vivo in response to CS.

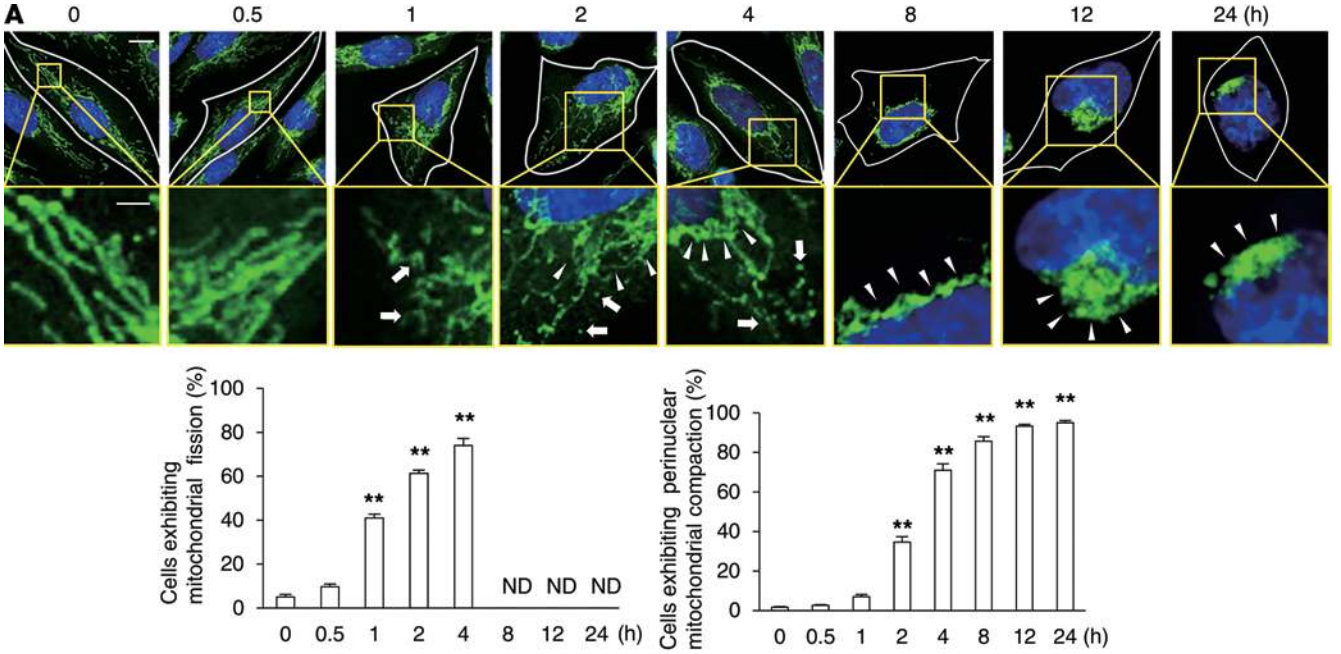
A
0
0.5
1
2
4
8
12
24 (h)
Cells exhibiting mitochondrial fission (%)
Cells exhibiting perinuclear mitochondrial compaction (%)
ND ND ND
**

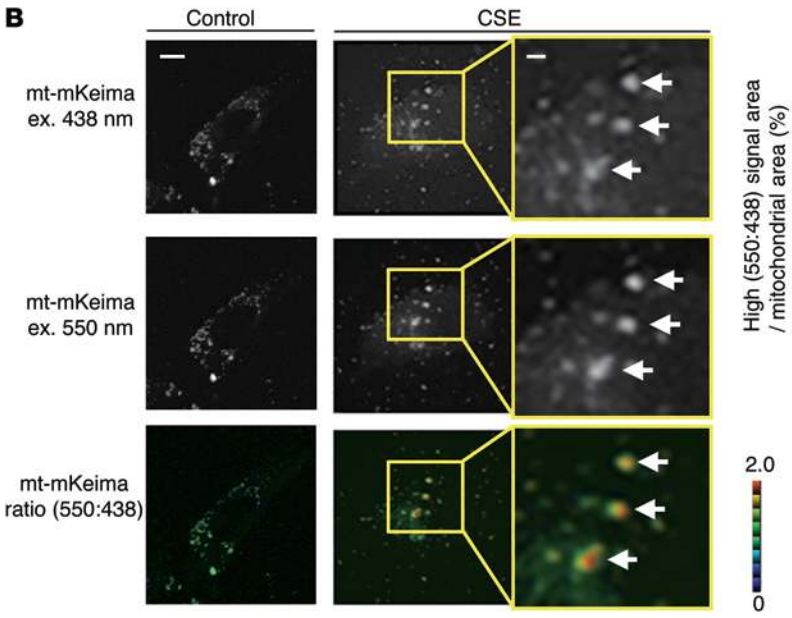
B
Control
CSE
mt-mKeima ex. 438 nm
mt-mKeima ex. 550 nm
mt-mKeima ratio (550:438)
2.0
0
High (550:438) signal area / mitochondrial area (%)
Control
CSE
**

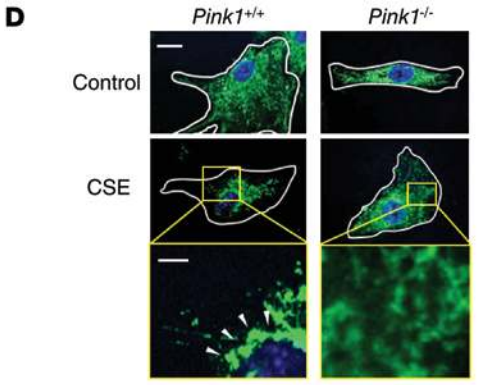
D
Pink1+/+
Pink1-/-
Control
CSE

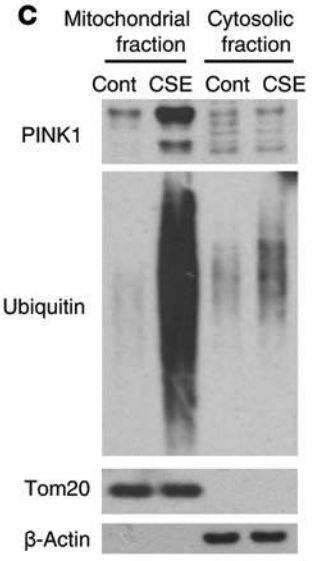
C
Mitochondrial fraction
Cytosolic fraction
Cont CSE Cont CSE
PINK1
Ubiquitin
Tom20
β-Actin

Figure 3. CSE induces mitophagy in pulmonary epithelial cells, which is regulated by PINK1. (**A**) Representative mitochondrial morphology (original magnification, ×120) in Beas-2B cells treated with 20% CSE for the indicated times. Blue: Hoechst 33258 (nucleus), green: Tom20 (mitochondria) (**A** and **D**). Scale bars: 10 μm (**A**, **B**, and **D**). Areas outlined in yellow are enlarged in lower panels and in panels at right (scale bars: 2 μm) (**A**, **B**, and **D**). Cell border is outlined in white (**A** and **D**). White arrows show mitochondrial fission, and white arrowheads show perinuclear compaction of mitochondria (**A** and **D**). Histograms show quantification of cells exhibiting fission or perinuclear mitochondrial compaction. 100 cells per group were analyzed in 3 independent experiments. (**B**) Cumulative detection of mitophagy using mt-mKeima (original magnification, ×120). Beas-2B cells were transfected with mt-mKeima and treated with 20% CSE for 8 hours. Pseudo-red color indicates acidic puncta. Histogram shows the ratio of high (550:438) signal area (red) to total mitochondrial area. 30 cells per group were analyzed in 3 independent experiments. ex., excitation. (**C**) Beas-2B cells were treated with 20% CSE for 6 hours, followed by mitochondrial fractionation. Immunoblot analysis of PINK1 and ubiquitin in mitochondrial/cytosolic fractions. (**D**) Representative mitochondrial morphology (original magnification, ×144) in alveolar epithelial cells isolated from *Pink1*$^{+/+}$ or *Pink1*$^{-/-}$ mice treated with 20% CSE for 4 hours. Image is representative of 5 images/slide; n = 3 slides/condition (**A**, **B**, and **D**). Data represent the mean ± SEM (**A** and **B**). $^{**}P < 0.01$ by unpaired, 2-tailed Student's t test (**A** and **B**) versus control (**A**).

PINK1-null mice and Mdivi-1–treated mice are protected against disruption of airway function during subchronic CS exposure. To examine the physiological function of mitophagy in experimental COPD, we used a mouse model of airway MCC after CS exposure. We measured MCC using whole-mouse, single-photon emission computed tomographic (μSPECT) imaging following an oropharyngeal aspiration procedure in which the radiopharmaceutical ^{99m}technetium-sulfur colloid (^{99m}Tc-SC) was instilled into mouse lungs (8, 35). We assessed the MCC function of *Pink1*$^{-/-}$ or *Pink1*$^{+/+}$ littermate mice exposed to CS for 3 weeks (Figure 8A). Consistent with our previous studies in wild-type C57BL/6 mice (8), the efficacy of clearance of ^{99m}Tc-SC from wild-type *Pink1*$^{+/+}$ mouse lungs exposed to CS was significantly reduced compared with that in air-exposed controls, indicative of impaired MCC function. *Pink1*$^{-/-}$ mice were significantly protected from CS-impaired MCC relative to *Pink1*$^{+/+}$ mice (Figure 8A). Injection of Mdivi-1 also ameliorated CS-dependent impairment of MCC relative to that seen in vehicle-treated mice after 3 weeks of CS exposure (Figure 8B). These results suggest that PINK1 contributes to a pathogenic process leading to airway dysfunction in the subchronic CS exposure model, and this process can be reversed by a chemical inhibitor of mitophagy.

Genetic deficiency in PINK1 protects against CS-induced airspace enlargement in vivo in an emphysema model. To further examine the physiological function of mitophagy in pathological processes associated with COPD, we used a mouse model of emphysema, in which *Pink1*$^{-/-}$ mice or corresponding wild-type mice were subjected to CS exposure for 6 months and their lungs analyzed for airspace enlargement using the mean chord length (see Methods). Wild-type mice exposed to CS displayed significantly increased airspace in the lung relative to that seen in RA-treated controls (Figure 8, C and E). In contrast, we did not observe airspace enlargement in CS-exposed *Pink1*$^{-/-}$ mouse lungs (Figure 8, C and D). Interestingly, *Park2*$^{-/-}$ mouse lungs showed similar airspace enlargement compared with that in lungs from wild-type mice (Figure 8, E and F). These results suggest that PINK1, but not Parkin, contributes to a pathogenic process leading to airspace enlargement/emphysema in the chronic CS exposure model.

Mitophagy and necroptosis factors can be detected in vivo in an emphysema model. We next assessed the temporal and spatial expression of mitophagy and necroptosis factors and their relevance to pathogenic changes in the mouse lung in the chronic CS exposure model. We examined the expression of p-Drp1 (Ser616), LC3B, and RIP3 in the lungs of mice exposed to RA or CS for 3 weeks, 3 months, and 6 months. We found that expression of p-Drp1 increased after 3 weeks of CS exposure (Figure 9A) and that expression of LC3B and RIP3 increased after 3 months of CS exposure (Figure 9, A and B). Consistent with immunoblot analysis, increased LC3B and RIP3 staining occurred in epithelial cells after 3 months of CS exposure (Figure 9C). Interestingly, we detected high levels of RIP3 staining near emphysematous regions, whereas LC3B showed diffuse staining in the lung.

Next, to evaluate the effect of CS on mitochondrial integrity in vivo, we counted swollen mitochondria with evidence of severely disrupted cristae in the mouse lungs following exposure to RA or CS, as detected by electron microscopy (Figure 9D). The percentage of abnormal mitochondria in lung tissue was significantly increased after 3 months of CS exposure.

Mitophagy and necroptosis factors can be detected in human COPD lung. Finally, to ascertain the relevance of our in vitro and in vivo observations in human disease, we assessed the relative expression of mitophagy and necroptosis factors in human lungs from either control or COPD patients (see Supplemental Table 1 for clinical information). We found that expression of PINK1, RIP3, and Drp1 was increased in lung tissue homogenates from COPD patients relative to that in control subjects (Figure 10A). Furthermore, we observed that increased PINK1 and RIP3 staining occurred in the epithelial cells of COPD patients relative to that seen detected in control subjects (Figure 10, B and C). Confocal imaging revealed increased expression and coincidence of PINK1 and RIP3 expression in COPD lungs relative to that observed in control subjects (Figure 10D). The release of HMGB1, a marker of necrosis, into plasma of COPD patients was higher than in healthy controls (Supplemental Figure 3D). These observations in human clinical tissue strongly suggest that our experimental data associating mitophagy with necroptosis is relevant to human disease.

Discussion

An accumulating body of evidence suggests that autophagy is relevant to human diseases (36–38). In addition to turnover of organelles and proteins, autophagy can influence fundamental processes, including inflammatory and immune responses, host defense, metabolic pathways, and programmed cell death. The role of autophagy in disease pathogenesis is complex and may involve adaptive or maladaptive outcomes. We previously observed increased autophagosome numbers and increased expression of LC3B-II, the active form of LC3B, in human lung specimens from patients with COPD (6). Genetic deletion of specific autophagy proteins reduced airspace enlargement in an in vivo emphysema model and protected against disruption of

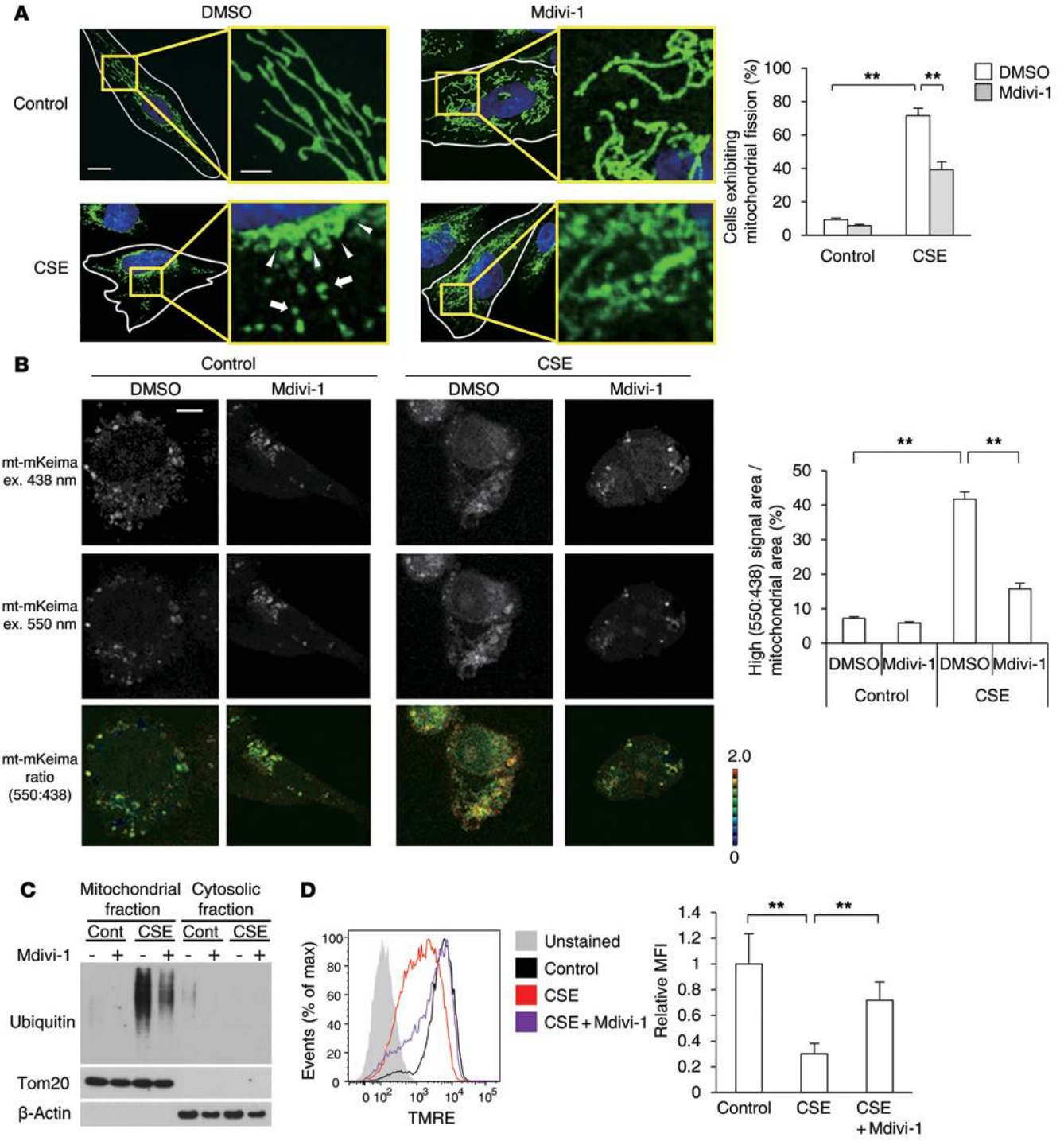

Figure 4. Mdivi-1 reduces CSE-induced mitophagy and loss of $\Delta\Psi_m$. (**A**) Representative mitochondrial morphology (original magnification, ×120) in Beas-2B cells incubated for 3 hours with Mdivi-1 (50 μM) or vehicle (DMSO) and treated with 20% CSE for 4 hours. Blue: Hoechst 33258 (nucleus); green: Tom20 (mitochondria). Scale bar: 10 μm (**A** and **B**). Right panels show enlargement of the yellow-framed areas (scale bar: 2 μm). White outline delineates cell borders. White arrows and arrowheads show mitochondrial fission and perinuclear compaction, respectively. Histogram shows quantification of cells exhibiting mitochondrial fission. Image is representative of 5 images/slide; *n* = 3 slides/group (**A** and **B**). (**B**) Cumulative detection of mitophagy (original magnification, ×120). Beas-2B cells transfected with mt-mKeima were incubated with Mdivi-1 (50 μM) or vehicle (DMSO) and treated with 20% CSE for 8 hours. Histogram shows quantification of the ratio of high (550:438) signal area to total mitochondrial area. 30 cells/group were analyzed in 3 independent experiments. (**C**) Immunoblot analysis of ubiquitin in mitochondrial/cytosolic fractions of Beas-2B cells incubated with Mdivi-1 (50 μM) or vehicle (DMSO) and treated with 20% CSE for 6 hours. (**D**) Flow cytometry of Beas-2B cells labeled with TMRE. Beas-2B cells incubated with Mdivi-1 (50 μM) or vehicle (DMSO) were treated with 20% CSE for 4 hours. The *x* axis shows the fluorescent signal intensity, and the *y* axis represents the cell number normalized as a percentage of the maximum (% of max). Data are representative of 3 experiments. Data represent the mean ± SEM (**A**, **B**, and **D**). $^{**}P < 0.01$ by unpaired, 2-tailed Student's *t* test (**A**, **B**, and **D**).

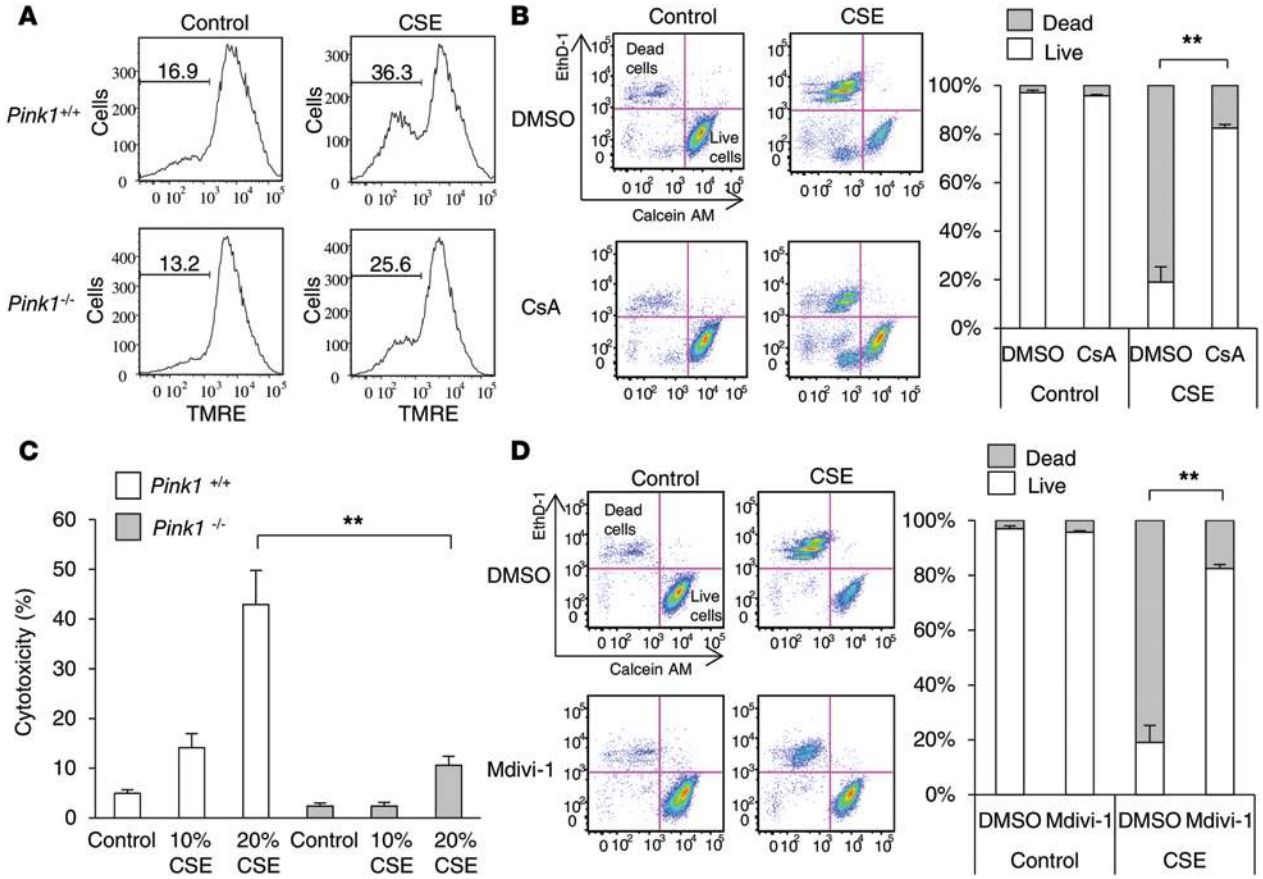

Figure 5. CSE-induced mitophagy decreases $\Delta\Psi_m$, leading to cell death in pulmonary epithelial cells. (**A**) Flow cytometry of alveolar epithelial cells obtained from *Pink1*$^{-/-}$ and *Pink1*$^{+/+}$ mice. Alveolar epithelial cells were treated with 20% CSE for 4 hours and labeled with TMRE. The *x* axis shows the fluorescent signal intensity of TMRE, and the *y* axis shows the cell number with corresponding fluorescence intensity. Numbers above bracketed lines indicate the percentage of cells with loss of mitochondrial membrane potential. Data are representative of 2 experiments. (**B**) Beas-2B cells were incubated for 1 hour with CsA (10 μM) or vehicle (DMSO) and treated with 20% CSE for 15 hours. Cell death was determined by calcein AM/EthD-1 flow cytometry. The *x* axes show calcein AM staining, and the *y* axes show EthD-1 staining (**B** and **D**). Data are representative of 3 independent experiments. (**C**) Alveolar epithelial cells were obtained from *Pink1*$^{-/-}$ and *Pink*$^{+/+}$ mice. Alveolar epithelial cells were treated with 10% or 20% CSE for 15 hours. Cytotoxicity was measured by LDH release. Data are representative of 2 experiments. (**D**) Beas-2B cells were incubated for 3 hours with Mdivi-1 (50 μM) or vehicle (DMSO) and treated with 20% CSE for 15 hours. Cell death was determined by calcein AM/EthD-1 flow cytometry. Data are representative of 3 experiments. Data represent the mean ± SEM (**B**–**D**). $^{**}P < 0.01$ by unpaired, 2-tailed Student's *t* test (**B**–**D**).

airway function during subchronic CS exposure; however, the underlying mechanisms have yet to be elucidated (5, 6, 8). These results, taken together, suggest a propathogenic role for autophagy in CS-induced emphysema.

Autophagy can selectively degrade specific proteins, organelles, and invading bacteria in processes referred to as "selective autophagy" (9–11, 39). Mitophagy, the specific autophagic elimination of mitochondria, may have relevance to clinical diseases (40). Here, we have shown that mitophagy occurs in epithelial cells subjected to CSE in association with mitochondrial dysfunction and that this process depends on PINK1 stabilization.

Generally, mitophagy in combination with altered mitochondrial dynamics is thought to serve as an intrinsic mitochondrial quality control mechanism. Mitochondrial fusion is important for the dissipation of metabolic energy and for the complementation of mitochondrial DNA gene products in heteroplasmic cells, whereas damaged mitochondria are separated from the mitochondrial network by fission and subsequently degraded by mitophagy (11, 41). Recent studies suggest that the process of mitophagy involves mitochondrial fission proteins (42). The GTPase Drp1, a core regulatory molecule for fission, relocalizes from a diffuse cytoplasmic distribution to a punctate mitochondrial distribution depending on its phosphorylation state, and subsequently mitochondrial fission occurs (43). In adult cardiac myocytes, overexpression of the dominant-negative form of Drp1 results in decreased mitochondrial fission and mitophagy (44). Mild oxidative stress specifically triggers mitophagy in a Drp1-dependent manner (45). Recent studies have applied Mdivi-1, a pharmacological inhibitor of Drp1, for the study of mitophagy (28–31). Here, we confirmed that CSE regulated Drp1 in pulmonary epithelial cells. Furthermore, we have shown that Mdivi-1 specifically reduced mitophagy, using the mt-mKeima assay, and inhibited mitochondrial ubiquitination.

In this study, we observed that significant mitochondrial depolarization occurred in pulmonary epithelial cells in response to CSE. Since mitochondrial uncouplers (e.g., carbonyl cyanide *m*-chlorophenyl hydrazine [CCCP]), which mimic mitochondrial

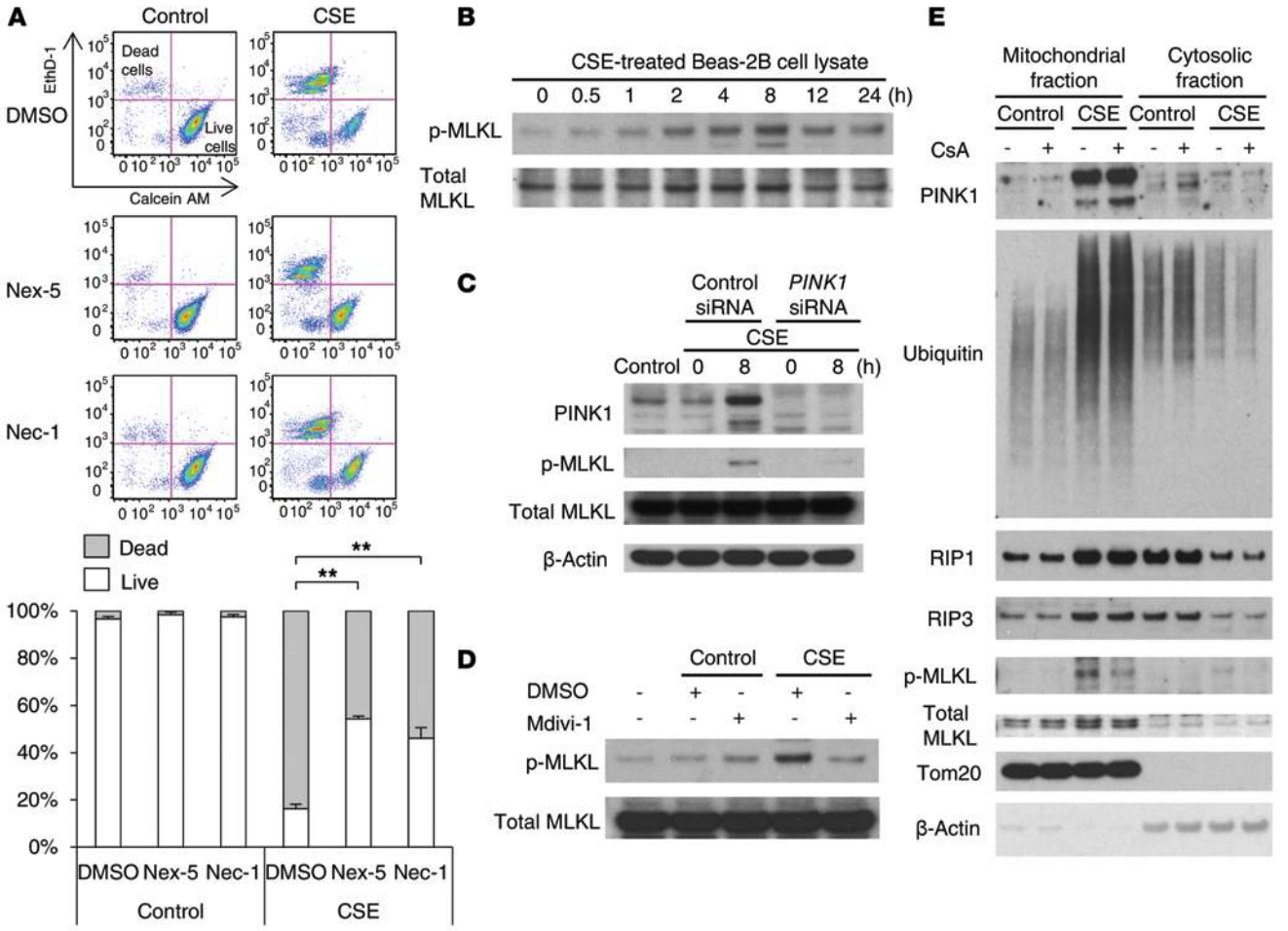

Figure 6. Mitophagy regulates CSE-induced necroptosis through loss of $\Delta\Psi_m$ in pulmonary epithelial cells. (**A**) Beas-2B cells were incubated for 1 hour with Nex-5 (30 μM), Nec-1 (50 μM), or vehicle (DMSO) and treated with 20% CSE for 15 hours. Cell death was determined by calcein AM/EthD-1 flow cytometry. The *x* axes show calcein AM staining, and the *y* axes show EthD-1 staining. Data are representative of 3 experiments. (**B**) Immunoblot analysis of p-MLKL (Thr357) and total MLKL in lysates obtained from Beas-2B cells treated with 20% CSE at the indicated times. (**C**) Beas-2B cells were pretreated with control siRNA or *PINK1* siRNA for 48 hours prior to treatment with 20% CSE for 8 hours. Cell lysates were immunoblotted for PINK1 and p-MLKL. Total MLKL and β-actin served as the standards. (**D**) Immunoblot analysis of p-MLKL and total MLKL. Beas-2B cells were incubated for 3 hours with Mdivi-1 (50 μM) or vehicle (DMSO) and treated with 20% CSE for 8 hours. Total MLKL served as the standard. (**E**) Beas-2B cells were incubated for 1 hour with CsA (10 μM) or vehicle (DMSO) and treated with 20% CSE for 6 hours. Mitochondrial/cytosolic fractions were immunoblotted for PINK1, ubiquitin, RIP1/3, p-MLKL, and MLKL. β-Actin and Tom20 served as the standards. Data represent the mean ± SEM (**A**). $^{**}P < 0.01$ by unpaired, 2-tailed Student's *t* test (**A**).

damage by decreasing $\Delta\Psi_m$, induce accumulation of PINK1 and recruitment of Parkin to mitochondria, mitochondrial dysfunction is considered an initiating event for mitophagy (11, 46, 47); however, this remains controversial (48). A recent study investigated the cellular fate of mitochondria damaged by the action of oxidative phosphorylation inhibitors, including CCCP, and suggested that mitophagy is not directly induced by mitochondrial damage (48, 49). It has also been reported that expression of unfolded proteins in the matrix causes accumulation of PINK1, resulting in activation of mitophagy independently of the loss of $\Delta\Psi_m$ (50). Consistent with these observations, we found that CsA, which prevented loss of $\Delta\Psi_m$ in CSE-treated cells, had no effect on CSE-induced PINK1 or ubiquitin expression in the mitochondria. A recent study has shown that ROS can regulate mitophagy in neurons (51). Mild oxidative stress triggers mitophagy in a Drp1-dependent manner (45). Furthermore, in bronchial epithelial cells, CSE-induced mitochondrial fragmentation is regulated by mtROS (52). Consistent with these reports, we found that MitoQ, a known mitochondria-targeted antioxidant, reduced CSE-induced PINK1 stabilization and phosphorylation of Drp1 on Ser616. We also observed the temporal dynamics of the correlation between mtROS, the phosphorylation of Drp1, and PINK1 stabilization. Our data suggest that CSE can promote mtROS production and phosphorylation of Drp1, which precede PINK1 stabilization and loss of $\Delta\Psi_m$.

Interestingly, we observed that genetic deficiency in *Pink1*, as well as Mdivi-1 treatment, protected against loss of $\Delta\Psi_m$ in response to CSE. These results suggest that activation of mitophagy is associated with a decline of mitochondrial membrane integrity in our model. We also assessed whether genetic deficiency in PINK1 can alter loss of $\Delta\Psi_m$ in response to stimulation with exogenous ROS. While H_2O_2 caused mitochondrial depolarization, we observed no significant difference between *Pink1*$^{+/+}$ and *Pink1*$^{-/-}$ cells. These results suggest that the mitophagy protein PINK1 potentially con-

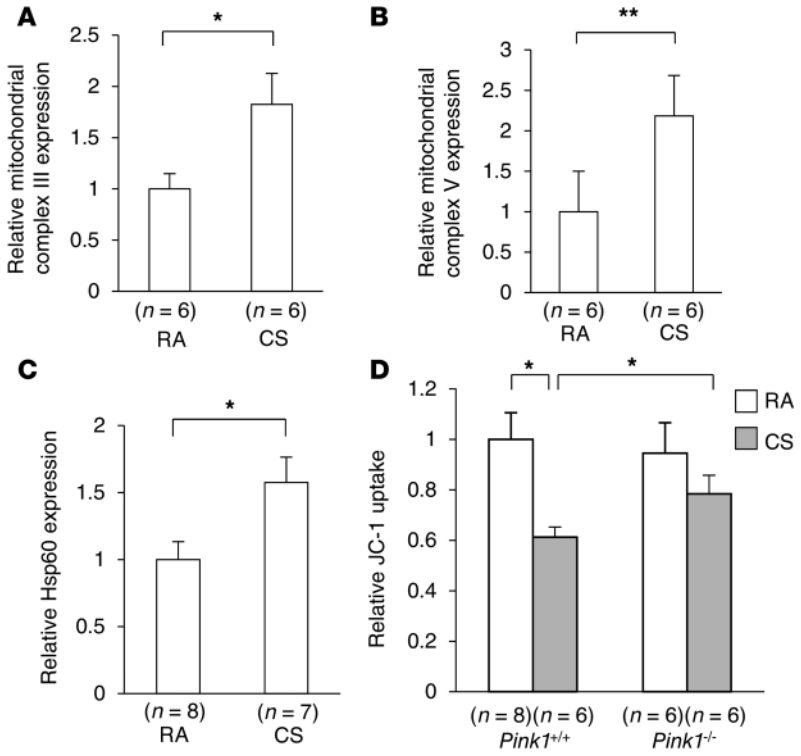

Figure 7. CS-induced mitophagy contributes to loss of $\Delta\Psi_m$ in vivo. Autophagosome/lysosome-enriched fractions of lungs from LC3B-GFP mice exposed to RA or CS for 3 weeks and immunoprecipitated with anti-GFP. GFP-immunoprecipitated LC3B-positive fractions were immunoblotted for the mitochondrial proteins complex III (**A**), complex V (**B**), and Hsp60 (**C**). (**D**) Mitochondrial functionality was studied by measuring JC-1 uptake in a mitochondria-enriched fraction of *Pink1*$^{+/+}$ and *Pink1*$^{-/-}$ mouse lungs following exposure to RA or CS for 6 months. All data represent the mean ± SEM. $^*P < 0.05$ and $^{**}P < 0.01$ by unpaired, 2-tailed Student's *t* test (**A**, **B**, and **C**) or by 2-way ANOVA with Bonferroni's post tests (**D**).

tributes to mitochondrial depolarization during CSE exposure, but not in response to exogenous ROS. Although it is commonly accepted that mitochondrial dysfunction initiates mitophagy, our results support a hypothesis that, in the specific context of CSE-induced cell stress, activated mitophagy aggravates mitochondrial injury and depolarization. Emerging studies have suggested that mitophagy may be deleterious in a context-specific manner (15). Clinical observations have suggested that oxidative stress correlated with abnormal mitochondrial function in the muscles of COPD patients (53, 54). We conclude that mitophagy may contribute to the CS-dependent degradation of the mitochondrial network, leading to unrecoverable loss of cellular integrity.

Previous studies have suggested that the treatment with zVAD, a pan-caspase inhibitor with broad specificity, induced autophagy and the death of L929 cells, and this cell death process required RIP1, suggesting that autophagy is involved in necroptosis (33). In several models, autophagy has been shown to regulate necroptosis (55, 56). In endothelial cells, inhibition of autophagy rescued palmitic acid–induced necroptosis (57). An emerging hypothesis, therefore, is that mitophagy also contributes to cell death in a context-specific fashion. Specifically, ceramide-initiated cell death required mitophagy, involving LC3-ceramide interactions at the mitochondria (15). During starvation, cell viability is sustained by sparing autophagic degradation of mitochondria through mitochondrial elongation (58). Although published studies indicated a relationship between necroptosis and disintegration of mitochondria, the precise mechanisms remain to be elucidated (18). Several reports have implicated mitochondria as downstream effectors of necrosome activation (59, 60). However, a recent study showed that necrosome activation does not require the intermediation of mitochondria to lead to cell death induced by ligands such as tumor necrosis factor (61). We found that CSE-induced MLKL phosphorylation, a RIP3-dependent process, was decreased in *PINK1*-knockdown cells and Mdivi-1–treated Beas-2B cells. In contrast, Nec-1, a necrosome inhibitor, had no effect on CSE-induced PINK1 expression. These data suggest that PINK1-dependent mitophagy, in response to CSE, can act as an upstream regulator of the necrosome.

In this study, we have also shown increased expression of p-Drp1 and increased accumulation of mitochondrial proteins in LC3B-immunoprecipitated LE fractions obtained from lung tissues from mice exposed to CS for 3 weeks. Furthermore, we observed that impaired mitochondrial integrity and expression of LC3B and RIP3 increased after 3 months of CS exposure. These results raise the possibility that pulmonary mitophagy begins as soon as 3 weeks after CS exposure in vivo; however, it may require 3 months to increase the mitophagic process to sufficiently impair mitochondria and induce necroptosis. Immunohistochemical analysis of lung tissue from mice exposed to CS for 3 months or 6 months revealed high expression of RIP3 staining near emphysematous regions, in contrast to high expression of LC3B in diffuse alveolar regions. Given that mitophagy may be active in the region with high expression of RIP3, it is possible for CS to induce mitophagy and general autophagy with spatial dispersion in the alveolar region of the lung.

Consistent with a pathogenic role for mitophagy in CS-dependent responses, we found that *Pink1*$^{-/-}$ mice were resistant to emphysema after CS exposure. Furthermore, we have shown that PINK1 contributes to mitochondrial depolarization in vivo in response to CS. In the emphysema model, it is possible that mitophagy-dependent cell death plays a role in lung tissue loss. This hypothesis is supported by our in vitro findings that active mitophagy promotes necroptosis in epithelial cells as well as by our observation that RIP3 staining is markedly enhanced in emphysematous tissue. In this study, we also observed that *Pink1*$^{-/-}$ mice and chemical inhibition of mitochondrial division/mitophagy using Mdivi-1 conferred protection against CS-induced disruption of airway function; however, the role of cell death in this process remains unclear at present. We cannot completely exclude the possibility that PINK1 participates in signaling pathways independently of its role in regulating mitophagy, which in turn may influence the progression of airway and

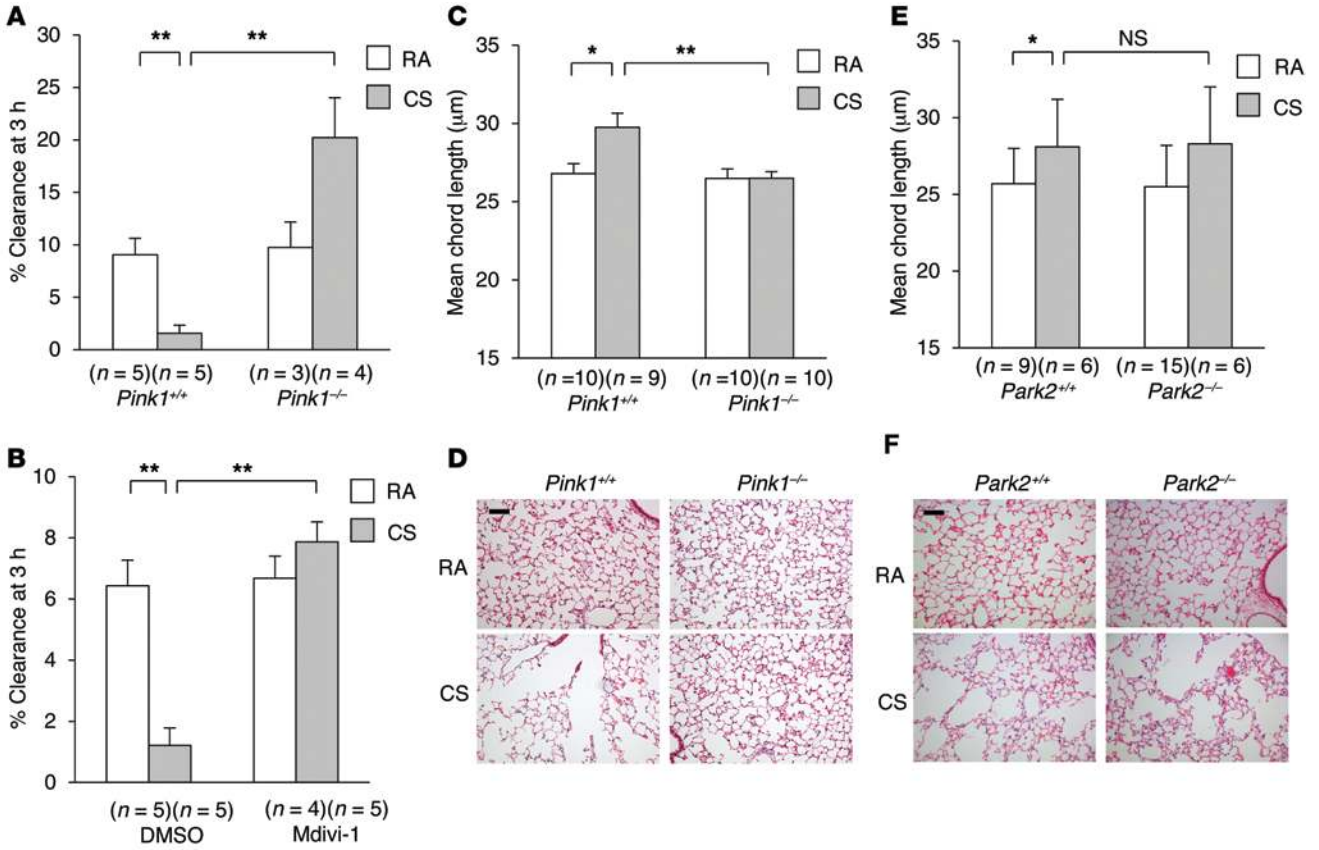

Figure 8. Mitophagy contributes to disruption of airway function and airspace enlargement during CS exposure in vivo. (**A**) MCC was assessed at 3 hours in *Pink1*$^{+/+}$ and *Pink1*$^{-/-}$ mice following exposure to RA or CS for 3 weeks. (**B**) MCC was assessed at 3 hours in mice i.p. injected with 50 mg/kg Mdivi-1 or vehicle (DMSO) 1 hour prior to exposure to CS Mice were exposed to RA or CS for 3 weeks. (**C**–**F**) Mice were exposed to RA or CS for 6 months. Chord lengths were measured in *Pink1*$^{+/+}$ and *Pink1*$^{-/-}$ mouse lungs (**C**) or in *Park2*$^{+/+}$ and *Park2*$^{-/-}$ mouse lungs (**E**). Chord lengths in *Pink1*$^{+/+}$ and *Pink1*$^{-/-}$ mouse lungs were calculated from a total of 2 independent CS exposure experiments. Representative images (original magnification, ×200) of *Pink1*$^{+/+}$ and *Pink1*$^{-/-}$ mouse lungs (**D**) or of *Park2*$^{+/+}$ and *Park2*$^{-/-}$ mouse lungs (**F**) are shown with modified H&E staining. Scale bar: 50 μm. Image is representative of 5 images/mouse; *n* = 3 mice/group. All data represent the mean ± SEM (**A**–**C** and **E**). **P* < 0.05 and ***P* < 0.01 by 2-way ANOVA with Bonferroni's post tests (**A**–**C** and **E**).

emphysematous phenotypes. Several molecules that regulate autophagy (e.g., p53, p62, beclin 1, LC3) have been shown to interact with other signaling platforms outside of their direct role in the autophagic pathway (62–64). It is therefore reasonable to speculate that PINK1, which is a serine/threonine kinase, may have potential for regulatory crosstalk with other signaling pathways outside of its role in mitophagy. Further elucidation of potential nonmitophagic pathways affected by PINK1 is beyond the scope of the current study. Nevertheless, our finding that the airway phenotype of *Pink1*$^{-/-}$ mice can be replicated by application of Mdivi-1 provides strong supporting evidence for a role of functional mitophagy in the pathogenic process.

As the majority of substrates of selective autophagy are ubiquitinated, ubiquitin functions as a general tag for selective autophagy in mammalian cells (9, 10). Although mitochondrial ubiquitination increased after CSE treatment, we found virtually no mRNA or protein expression of Parkin, the E3 ubiquitin ligase identified as a key regulator of neuronal mitophagy, in pulmonary epithelial cells. *PARK2* mRNA, however, was detected at low levels in whole-lung tissue. Furthermore, *Park2*$^{-/-}$ mice displayed no phenotype in the CS-induced emphysema model. Published studies showed that Parkin overexpression was needed to facilitate clearance of mitochondria, yet PINK1 could induce mitophagy independently of Parkin overexpression in the same cell line (46, 47). Several previous investigations are suggestive of PINK1-dependent, but Parkin-independent, mitophagy. Fu et al. have shown that Gp78 overexpression causes mitophagy that is dependent on PINK1 but not on Parkin (65). *Pink1*$^{-/-}$ mice were found to be resistant to *Staphylococcus*-induced acute lung injury. PINK1 was found to interact with an alternative ubiquitin E3 ligase component, Fbxo15, which promoted mitochondrial instability in this model (66). At present, we can speculate on the existence of additional PINK1 targets and/or E3 ubiquitin ligases that may be important in the lung in the context of CS exposure, and this may be the subject of future studies.

In conclusion, our data demonstrating increased expression of the mitophagy protein PINK1, the necroptosis regulator RIP3, and the fission regulator Drp1 in COPD lung tissues further support our hypothesis that mitophagy and necroptosis contribute to COPD. Our study provides a mechanistic explanation for how CS can regulate cell death through initiation of mitophagy and necroptosis. These data suggest that mitophagy contributes to the pathogenesis of COPD. Strategies targeting this pathway, such as treatment with Mdivi-1, may lead to novel therapies for COPD.

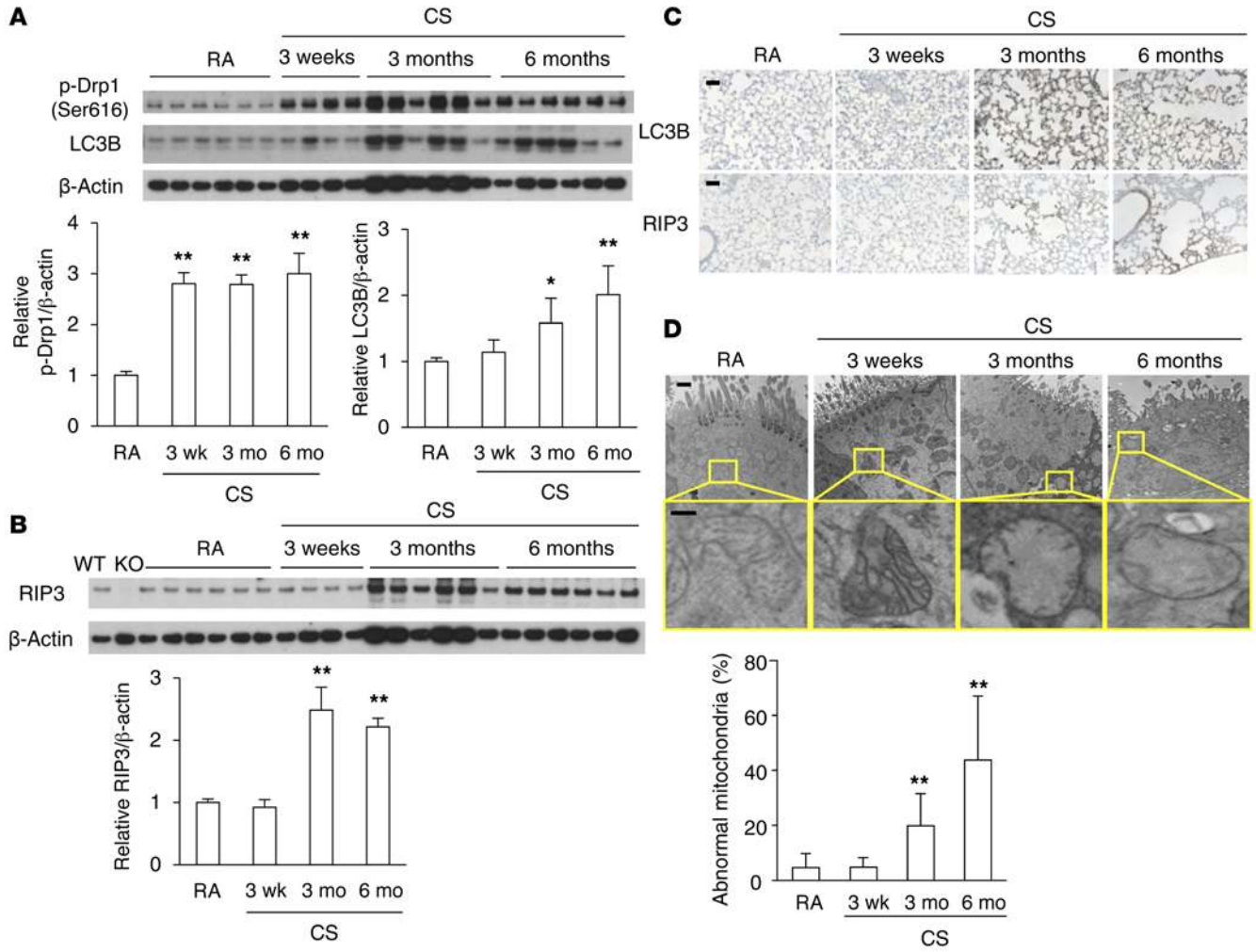

Figure 9. Mitophagy and necroptosis factors can be detected in mouse lung sections of the CS-exposure model. (**A** and **B**) Immunoblot analysis of p-Drp1 (Ser616), LC3B, and RIP3 from mouse lung homogenate samples following exposure to RA or CS for 3 weeks, 3 months, and 6 months. β-Actin served as the standard. p-Drp1 (Ser616), LC3B, and RIP3 expression was assessed by densitometry of immunoblots. Band intensities were normalized to β-actin. n = 4 or 6 samples/group. WT: *Ripk3*$^{+/+}$; KO: *Ripk3*$^{-/-}$. (**C**) Mouse lung sections following exposure to RA or CS for 3 weeks, 3 months, and 6 months were immunostained for LC3B or RIP3. Scale bar: 50 μm. Image (original magnification, ×200) is representative of 5 images/mouse; n = 4 mice/group. (**D**) Representative TEM images of mouse lung sections exposed to RA or CS for 3 weeks, 3 months, and 6 months. Scale bar: 500 nm. Mitochondria in yellow-outlined areas are shown enlarged in lower panels (scale bar: 100 nm). 10–20 images/treatment group; n = 1–3 mice/group. Histograms show quantification of abnormal mitochondria. Data were normalized to the RA control group for each time point. All data represent the mean ± SEM (**A**, **B**, and **D**). $^*P < 0.05$ and $^{**}P < 0.01$ versus control by unpaired, 2-tailed Student's t test (**A** and **B**) and 1-way ANOVA with Bonferroni's post tests (**D**).

Methods

Reagents. The following antibodies were used: rabbit antibody against human PINK1 (BC100-494; Novus Biologicals); rabbit antibody against human RIP1 (3493; Cell Signaling Technology); rabbit antibody against human RIP3 (ab56164; Abcam); goat antibody against human RIP3 (sc-47368; Santa Cruz Biotechnology Inc.); rabbit antibody against mouse RIP3 (AHP1797; AbD Serotec); mouse antibody against human β-actin (A2228; Sigma-Aldrich); rabbit antibody against human and mouse Tom20 (sc-11415; Santa Cruz Biotechnology Inc.); rabbit antibody against human p-Drp1 (3455; Cell Signaling Technology); mouse antibody against human Drp1 (611112, BD Transduction Laboratories; BD Biosciences); mouse monoclonal antibody against human ubiquitin (sc-8017; Santa Cruz Biotechnology Inc.); rabbit antibody against human p-MLKL (ABC234; EMD Millipore); rabbit antibody against human MLKL (M6697; Sigma-Aldrich); MitoProfile Total OXPHOS Rodent Western Blot antibody cocktail (ab110413; Abcam); mouse monoclonal antibody against Hsp60 (ab59457; Abcam); and rabbit antibody against human HMGB1 (3935; Cell Signaling Technology). Cyclosporine A was obtained from Sigma-Aldrich. Mdivi-1, Nec-1, and Nex-5 were purchased from Enzo Life Sciences. MitoQ was purchased from BIOTREND Chemicals.

Animals. All animal experimental protocols were approved by the Harvard Standing Committee for Animal Welfare. *Pink1*$^{-/-}$ and *Park2*$^{-/-}$ mice were provided by Jie Shen (Center for Neurologic Diseases, Brigham and Women's Hospital, Harvard Medical School). The generation of *Pink1*$^{-/-}$ and *Park2*$^{-/-}$ mice has been described (67–69). Lung tissue from *Ripk3*$^{-/-}$ mice that were used as a negative control for Western blot analysis were provided by V. Dixit and K. Newton (Genentech, South San Francisco, California, USA). LC3B-GFP mice were obtained from RIKEN BioResource Center (Ibaraki, Japan). C57BL/6 mice were purchased from The Jackson Laboratory.

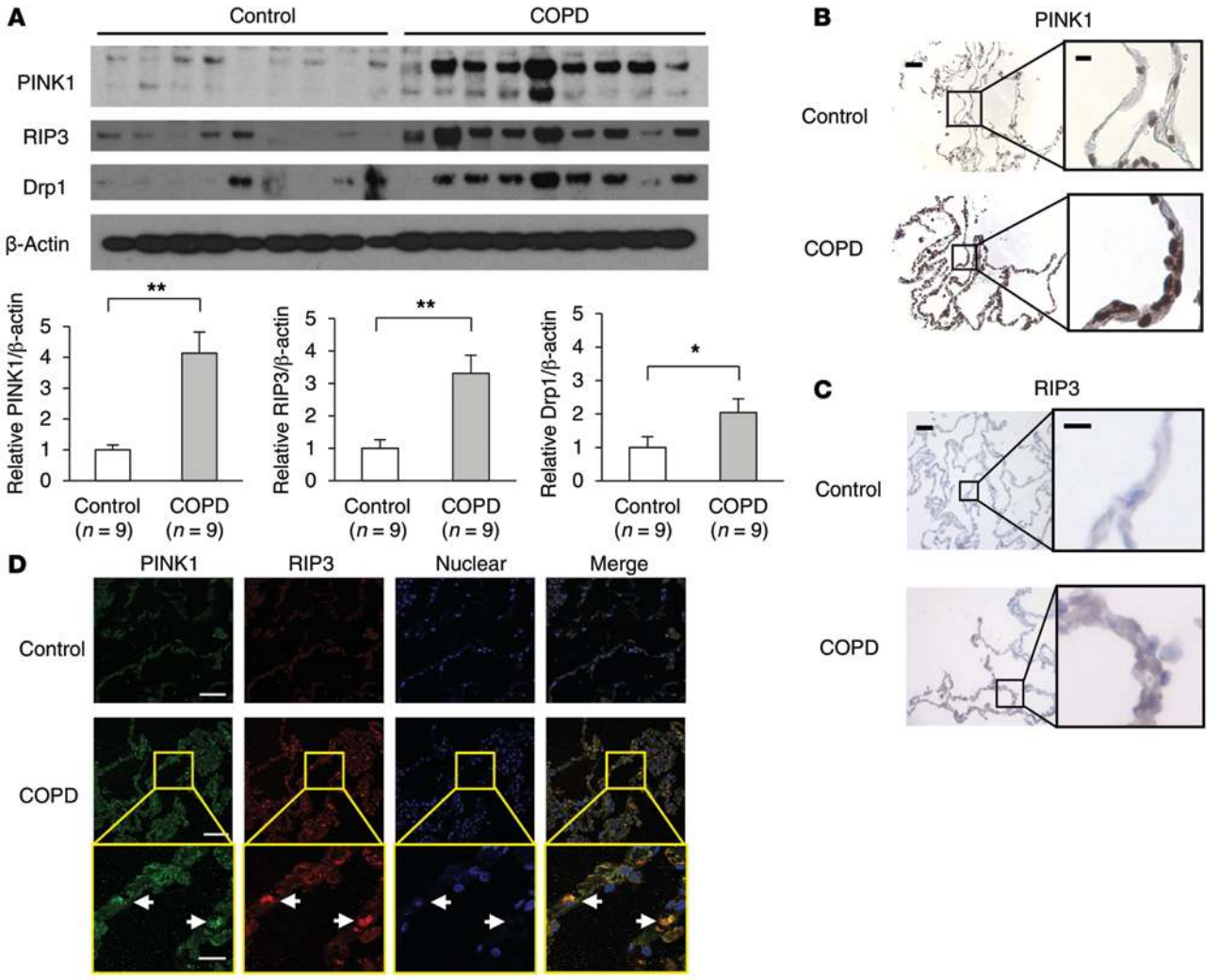

Figure 10. Mitophagy and necroptosis factors can be detected in human COPD lung. (**A**) Immunoblot analysis of PINK1, RIP3, and Drp1 in human lung homogenate samples from control subjects and COPD patients. β-Actin served as the standard. PINK1, RIP3, and Drp1 expression was assessed by densitometry of immunoblots. Band intensities were normalized to β-actin. $n = 9$ samples/group. Representative immunohistochemical study (original magnification, ×200) for PINK1 (**B**) or RIP3 (**C**) in human lung sections from never-smokers ($n = 3$ patients, 5 images/patient) or COPD patients ($n = 6$ patients, 5 images/patient). Scale bar: 100 μm. Outlined areas are shown enlarged at right (scale bar: 20 μm). (**D**) Immunofluorescence staining (original magnification, ×40) for PINK1 (green), RIP3 (red), and nuclear (blue) in human lung tissue from never-smokers ($n = 2$ patients, 3 images/patient) and COPD patients ($n = 2$ patients, 3 images/patient). Scale bar: 50 μm. Yellow-outlined areas are shown enlarged in bottom panels (scale bar: 10 μm). Data represent the mean ± SEM (**A**). $^{**}P < 0.01$ by unpaired, 2-tailed Student's *t* test (**A**).

In vivo CS and chemical treatments. Age-matched mice (6–12 weeks old) were exposed to RA or CS in whole-body exposure chambers as described (5) for 2 hours per day (150 mg/m^3), 5 days per week, for either 3 weeks, 3 months, or 6 months. Mdivi-1 was dissolved in DMSO and i.p. injected (50 mg/kg body weight) 5 days per week 1 hour prior to CS exposure. Control animals received vehicle (DMSO) injections.

Cell culture and CSE treatment. Primary HBE cells were obtained from ATCC and were cultured according to ATCC's instructions. Human lung bronchial epithelial Beas-2B cells were purchased from ATCC and maintained in DMEM containing 10% FBS and gentamicin (100 μg/ml). The primary alveolar epithelial cells of mouse lung were obtained as previously described and used for experiments before passage (70, 71). CSE was prepared and added to culture media as previously described (5, 6).

Mitochondria/cytosol fractionation in vitro. Mitochondria and cytosol were fractionated using the Mitochondria/Cytosol Fractionation Kit according to the manufacturer's protocol (Enzo Life Sciences).

Cytotoxicity assays. Cytotoxicity was assessed by measuring the release of LDH into the media (LDH-Cytotoxicity Colorimetric Assay Kit II; BioVision) according to the manufacturer's protocol.

Flow cytometry. To discriminate live and dead cells, cells were simultaneously stained with green fluorescent calcein-AM to indicate intracellular esterase activity and red fluorescent ethidium homodimer-1 to indicate loss of plasma membrane integrity using the LIVE/DEAD Viability/Cytotoxicity Kit (Molecular Probes). To assess the functional mitochondrial pool, cells were stained for 20 minutes at 37°C with 100 nM TMRE (Abcam), followed by CSE treatment. mtROS was measured in cells by MitoSOX (Invitrogen) staining (2.5 μM for 10 minutes at 37°C). Data were acquired with a

FACSCanto II (BD Biosciences) and analyzed with FlowJo analytical software (Tree Star Inc.).

Immunoblot analysis. Lysates were boiled for 10 minutes in NuPAGE sample-loading buffer (Invitrogen). Proteins were separated by electrophoresis through NuPAGE 4%–12% Bis-Tris gels (Invitrogen) and transferred to PVDF membranes or nitrocellulose membranes by electroblotting. For HMGB1 analysis in human plasma, human plasma samples were centrifuged at 20,000 *g* for 15 minutes at 4°C. Plasma (20 μl) was added to 80 μl NuPAGE sample-loading buffer. Samples containing 20 μg protein were used for electrophoresis.

HMGB1 analysis in the cell supernatant. Culture medium samples were briefly centrifuged and filtered to remove cellular debris. After centrifugation at 10,000 *g* for 10 minutes at 4°C, samples were concentrated by TCA-acetone precipitation. Proteins were separated by electrophoresis through NuPAGE 4%–12% Bis-Tris gels (Invitrogen) and transferred to PVDF membranes by electroblotting.

Immunohistochemical staining. Formalin-fixed, paraffin-embedded, 5-micron-thick lung sections were prepared. To perform immunohistochemical analysis, paraffin-embedded tissues were deparafinized in xylene, rehydrated, and retrieved by Immunosaver Antigen Retriever (64142; Electron Microscopy Sciences). Tissues were immunostained with rabbit antibody against human PINK1 (BC100-494; Novus Biologicals) and rabbit antibody against human RIP3 (ab56164; Abcam) using VECTASTAIN Elite ABC Kit (PK-6101; Vector Laboratories) according to the manufacturer's protocol. Mouse sections were stained with rabbit antibody against LC3B (Sigma-Aldrich; L7543) or rabbit antibody against mouse RIP3 (AHP1797; AbD Serotec).

Immunofluorescence staining. For cultured cells, after treatment, cells were fixed with 4% paraformaldehyde and analyzed with immunofluorescence staining by standard methods. Formalin-fixed, paraffin-embedded lung tissue sections were deparafinized in xylene, rehydrated, and retrieved by Immunosaver Antigen Retriever (64142; Electron Microscopy Sciences). Samples were viewed with a Zeiss LSM 510 META system (Carl Zeiss) equipped with a multiargon laser (458, 488, and 514.5 nm) and an He-Ne laser (543 nm). Mitochondrial morphology was judged as exhibiting fission if greater than 90% of the mitochondria in the cytoplasm outside of the perinuclear compaction were punctate or circular and as exhibiting perinuclear mitochondrial compaction if greater than 90% of mitochondria accumulated in the perinuclear area.

Confocal imaging of mitophagy. The mitochondria-targeted form of the mKeima ratiometric pH probe (mt-mKeima) was used as a sensitive and quantitative assessment of mitophagy (27). The mt-mKeima probe was obtained from H. Katayama and A. Miyawaki (RIKEN, Tokyo, Japan). Beas-2B cells were treated with CSE, fixed, and analyzed for mitophagy by confocal microscopy as previously described (25). Briefly, Beas 2B cells were transfected with mt-mKeima using Lipofectamine LTX with Plus Reagent (Life Technologies). After incubation for 42 hours, Beas-2B cells treated with 20% CSE for 8 hours were fixed with 4% paraformaldehyde and examined by confocal imaging using a Leica SP8 X Confocal Microscope. Ratio (550:438) images of mt-mKeima were created and analyzed using MetaMorph software. High (550:438) signal areas and mitochondrial areas were calculated, and the ratio (high [550:438] signal area/mitochondrial area) was used as an index of mitophagic activity.

Transmission electron microscopy. Beas 2B cells were fixed in 2.5% (vol/vol) glutaraldehyde after CSE treatment as previously described (6). Transmission electron microscopy (TEM) samples from mice were fixed in 2.5% (vol/vol) glutaraldehyde and embedded as previously described (6). The samples were imaged using a Technai G2 Spirit BioTWIN TEM. For electron microscopy quantification, 10–15 image fields were selected for each mouse or sample. To quantify abnormal mitochondria in the mouse lung, all mitochondria and swollen mitochondria with evidence of severely disrupted cristae were counted.

Metabolic assays. The OCR was measured in Beas-2B cells using a Seahorse XF96 analyzer (Seahorse Bioscience).

RNA-mediated interference. siRNA duplexes were obtained from Dharmacon. Beas-2B cells were plated on 6-well plates at a density of 8×10^4 cells per well and were transfected with siRNA (8 nM) using Lipofectamine RNAiMAX transfection reagent (Life Technologies).

Real-time qPCR. Total brain mRNA (636530; Clontech), trachea mRNA (636541; Clontech), and whole-lung mRNA (636524; Clontech) were reverse transcribed with SuperScript III Reverse Transcriptase (Life Technologies). For qPCR analysis of mRNA expression in HBE cells and Beas-2B cells, cDNA was prepared from the cells using the Cells to CT Kit (Ambion, Life Technologies) according to the manufacturer's protocol. TaqMan primers for human PINK1, human Parkin, and human β-actin for gene expression assays were purchased from Life Technologies. Real-time qPCR was carried out with an ABI PRISM 7300 Sequence Detection System using TaqMan PCR Master Mix (Life Technologies).

Isolation of autophagosomes from LC3B-GFP mice. A detailed protocol for the isolation of autophagosomes from LC3B-GFP mice has been described previously (8). Briefly, LC3B-GFP mice were exposed to CS or RA for 3 weeks. After lung tissues were flash-frozen, LC3B-positive autophagosomes and lysosomes were immunoprecipitated with GFP-conjugated μMACS microbeads (Miltenyi Biotec) using the magnetic field of a μMACS separator.

Mitochondrial isolation and measurement of $\Delta\Psi_m$ in vivo. A mitochondria-enriched fraction was obtained from 100 mg fresh lung specimens using the Mitochondria Isolation Kit (MITOISO1; Sigma-Aldrich) according to the manufacturer's protocol. $\Delta\Psi_m$ was evaluated by measuring uptake of JC-1 (J4519; Sigma-Aldrich). Fluorescence measurements were performed with a BioTek FLx800 fluorescence microplate reader.

Lung morphometry. Lung samples were processed for morphometric analysis, and airspace enlargement was quantified using the mean linear intercept (MLI) method as previously described (5, 6).

Assessment of MCC in vivo. MCC was quantified using a noninvasive, oropharyngeal aspiration procedure as previously described (8, 35). Briefly, Mice were anesthetized, and 50 μl normal saline containing approximately 0.3 to 0.5 mCi ^{99m}Tc-SC was introduced into the distal part of the oropharynx and aspirated. Mouse lungs were imaged immediately after aspiration (time: 0 hour), at 1 hour, and at 3 hours. Whole-mouse 3D μ-SPECT images from the 0-, 1-, and 3-hour time points were obtained, reconstructed, analyzed, and expressed as the percentage removed by MCC.

Patients. Patient samples were classified based on the guidelines of the Global Initiative for Obstructive Lung Disease (72). Patient samples were obtained from the Lung Tissue Research Consortium (LTRC). Control samples from transplant donors were obtained from

Brigham and Women's Hospital. Characteristics of the subjects are described in Supplemental Table 1.

Statistics. Data are presented as the mean ± SEM. Differences in measured variables between the experimental and control groups were assessed using an unpaired, 2-tailed Student's *t* test and between multiple groups and conditions using 2-way ANOVA and Bonferroni's post tests. For MCC assays, a significant *P* value was followed by a pairwise comparison using a 2-sample Student's *t* test for a priori hypotheses only. Thus, no adjustment in the significance level was made for multiple comparisons. *P* values were calculated, and minimum statistical significance was accepted at $P < 0.05$.

Study approval. All animal experimental protocols were approved by the Harvard Standing Committee for Animal Welfare (Harvard Medical School, Boston, Massachusetts, USA). All analysis of human tissue was approved by the IRB of Brigham and Women's Hospital and was carried out according to its guidelines. Informed consent was obtained directly from each subject and documented in writing before the start of study-related procedures. The written and oral information provided to subjects was approved by the Partners Human Research Committee (PHRC; Boston, Massachusetts, USA) before and during the informed consent process.

Acknowledgments

We thank I.O. Rosas, E. Ifedigbo, H.C. Lam, Z.H. Chen, and C.H. An for their technical assistance. This work was supported by NIH grants P01 HL114501-01 and P01 HL105339 (to A.M.K. Choi).

Address correspondence to: Augustine M.K. Choi, Joan and Sanford I. Weill Department of Medicine, Weill Cornell Medical Center, 525 East 68th Street, Room M-522, Box 130, New York, New York 10065, USA. Phone: 212.746.4720; E-mail: amc2056@med.cornell.edu.

1. Dal-Ré R. Worldwide behavioral research on major global causes of mortality. *Health Edu Behav*. 2011;38(5):433–440.
2. Barnes PJ. Chronic obstructive pulmonary disease. *New Engl J Med*. 2000;343(4):269–280.
3. Barnes PJ, Shapiro SD, Pauwels RA. Chronic obstructive pulmonary disease: molecular and cellular mechanisms. *Eur Resp J*. 2003;22(4):672–688.
4. Rabe KF, *et al*. Global strategy for the diagnosis, management, and prevention of chronic obstructive pulmonary disease: GOLD executive summary. *Am J Respir Crit Care Med*. 2007;176(6):532–555.
5. Chen ZH, et al. Autophagy protein microtubule-associated protein 1 light chain-3B (LC3B) activates extrinsic apoptosis during cigarette smoke-induced emphysema. *Proc Natl Acad Sci U S A*. 2010;107(44):18880–18885.
6. Chen ZH, et al. Egr-1 regulates autophagy in cigarette smoke-induced chronic obstructive pulmonary disease. *PLoS One*. 2008;3(10):e3316.
7. Mizushima N, Komatsu M. Autophagy: renovation of cells and tissues. *Cell*. 2011; 147(4):728–741.
8. Lam HC, et al. Histone deacetylase 6-mediated selective autophagy regulates COPD-associated cilia dysfunction. *J Clin Invest*. 2013;123(12):5212–5230.
9. Shaid S, Brandts CH, Serve H, Dikic I. Ubiquitination and selective autophagy. *Cell Death Differ*. 2013;20(1):21–30.
10. Ichimura Y, Komatsu M. Selective degradation of p62 by autophagy. *Semin Immunopathol*. 2010;32(4):431–436.
11. Youle RJ, Narendra DP. Mechanisms of mitophagy. *Nature Rev Mol Cell Biol*. 2011;12(1):9–14.
12. Kitada T, et al. Mutations in the parkin gene cause autosomal recessive juvenile parkinsonism. *Nature*. 1998;392(6676):605–608.
13. Springer W, Kahle PJ. Regulation of PINK1-Parkin-mediated mitophagy. *Autophagy*. 2011;7(3):266–278.
14. Green DR, Galluzzi L, Kroemer G. Mitochondria and the autophagy-inflammation-cell death axis in organismal aging. *Science*. 2011;333(6046):1109–1112.
15. Sentelle RD, et al. Ceramide targets autophagosomes to mitochondria and induces lethal mitophagy. *Nat Chem Biol*. 2012;8(10):831–838.
16. Slebos DJ, et al. Mitochondrial localization and function of heme oxygenase-1 in cigarette smoke-induced cell death. *Am J Respir Cell Mol Biol*. 2007;36(4):409–417.
17. Galluzzi L, et al. Molecular definitions of cell death subroutines: recommendations of the Nomenclature Committee on Cell Death 2012. *Cell Death Differ*. 2012;19(1):107–120.
18. Vandenabeele P, Galluzzi L, Vanden Berghe T, Kroemer G. Molecular mechanisms of necroptosis: an ordered cellular explosion. *Nat Rev Mol Cell Biol*. 2010;11(10):700–714.
19. Zhang DW, et al. RIP3, an energy metabolism regulator that switches TNF-induced cell death from apoptosis to necrosis. *Science*. 2009;325(5938):332–336.
20. He S, et al. Receptor interacting protein kinase-3 determines cellular necrotic response to TNF-α. *Cell*. 2009;137(6):1100–1111.
21. Galluzzi L, et al. Programmed necrosis from molecules to health and disease. *Int Rev Cell Mol Biol*. 2011;289:1–35.
22. Welz PS, et al. FADD prevents RIP3-mediated epithelial cell necrosis chronic intestinal inflammation. *Nature*. 2011;477(7364): 330–334.
23. Günther C, et al. Caspase-8 regulates TNF-α-induced epithelial necroptosis terminal ileitis. *Nature*. 2011;477(7364):335–339.
24. Twig G, et al. Fission and selective fusion govern mitochondrial segregation and elimination by autophagy. *EMBO J*. 2008;27(2):433–446.
25. Kashatus DF, Lim KH, Brady DC, Pershing NL, Cox AD, Counter CM. RALA and RALBP1 regulate mitochondrial fission at mitosis. *Nat Cell Biol*. 2011;13(9):1108–1115.
26. Orvedahl A, et al. Image-based genome-wide siRNA screen identifies selective autophagy factors. *Nature*. 2011;480(7375):113–117.
27. Katayama H, Kogure T, Mizushima N, Yoshimori T, Miyawaki A. A sensitive and quantitative technique for detecting autophagic events based on lysosomal delivery. *Chem Biol*. 2011;18(8):1042–1052.
28. Givvimani S, Munjal C, Tyagi N, Sen U, Metreveli N, Tyagi SC. Mitochondrial division/mitophagy inhibitor (Mdivi) ameliorates pressure overload induced heart failure. *PLoS One*. 2012;7(3):e32388.
29. Vazquez-Martin A, Cufi S, Corominas-Faja B, Oliveras-Ferraros C, Vellon L, Menendez JA. Mitochondrial fusion by pharmacological manipulation impedes somatic cell reprogramming to pluripotency: new insight into the role of mitophagy in cell stemness. *Aging*. 2012;4(6):393–401.
30. Zhang X, et al. Cerebral ischemia-reperfusion-induced autophagy protects against neuronal injury by mitochondrial clearance. *Autophagy*. 2013;9(9):1321–1333.
31. Gharanei M, Hussain A, Janneh O, Maddock H. Attenuation of doxorubicin-induced cardiotoxicity by mdivi-1: a mitochondrial division/mitophagy inhibitor. *PLoS One*. 2013;8(10):e77713.
32. Shen HM, Codogno P. Autophagic cell death: Loch Ness monster or endangered species? *Autophagy*. 2011;7(5):457–465.
33. Yu L, et al. Regulation of an ATG7-beclin 1 program of autophagic cell death by caspase-8. *Science*. 2004;304(5676):1500–1502.
34. Sun L, et al. Mixed lineage kinase domain-like protein mediates necrosis signaling downstream of RIP3 kinase. *Cell*. 2012;148(1–2):213–227.
35. Foster WM, Walters DM, Longphre M, Macri K, Miller LM. Methodology for the measurement of mucociliary function in the mouse by scintigraphy. *J Appl Physiol*. 2001;90(3):1111–1117.
36. Choi AM, Ryter SW, Levine B. Autophagy in human health and disease. *N Engl J Med*. 2013;368(7):651–662.
37. Levine B, Kroemer G. Autophagy in the pathogenesis of disease. *Cell*. 2008;132(1):27–42.
38. Rubinsztein DC, Codogno P, Levine B. Autophagy modulation as a potential therapeutic target for diverse diseases. *Nat Rev Drug Discov*. 2012;11(9):709–730.
39. Levine B, Mizushima N, Virgin HW. Autophagy in immunity and inflammation. *Nature*. 2011;469(7330):323–335.
40. Chen H, Chan DC. Mitochondrial dynamics — fusion, fission, movement, and mitophagy — in neurodegenerative diseases. *Hum Mol Genet*. 2009;18(R2):R169–R176.
41. Westermann B. Mitochondrial fusion and fission in cell life and death. *Nat Rev Mol Cell Biol*.

2010;11(12):872–884.
42. Otera H, Ishihara N, Mihara K. New insights into the function and regulation of mitochondrial fission. *Biochim Biophys Acta*. 2013;1833(5):1256–1268.
43. Smirnova E, Griparic L, Shurland DL, van der Bliek AM. Dynamin-related protein Drp1 is required for mitochondrial division in mammalian cells. *Mol Biol Cell*. 2001;12(8):2245–2256.
44. Lee Y, Lee HY, Hanna RA, Gustafsson ÅB. Mitochondrial autophagy by Bnip3 involves Drp1-mediated mitochondrial fission recruitment of Parkin in cardiac myocytes. *Am J Physiol Heart Circ Physiol*. 2011;301(5):H1924–H1931.
45. Frank M, et al. Mitophagy is triggered by mild oxidative stress in a mitochondrial fission dependent manner. *Biochim Biophys Acta*. 2012;1823(12):2297–2310.
46. Narendra DP, et al. PINK1 is selectively stabilized on impaired mitochondria to activate parkin. *PLoS Biology*. 2010;8(1):e1000298.
47. Narendra D, Tanaka A, Suen DF, Youle RJ. Parkin is recruited selectively to impaired mitochondria and promotes their autophagy. *J Cell Biol*. 2008;183(5):795–803.
48. Bhatia-Kissova I, Camougrand N. Mitophagy is not induced by mitochondrial damage but plays a role in the regulation of cellular autophagic activity. *Autophagy*. 2013;9(11):1897–1899.
49. Padman BS, Bach M, Lucarelli G, Prescott M, Ramm G. The protonophore CCCP interferes with lysosomal degradation of autophagic cargo in yeast and mammalian cells. *Autophagy*. 2013;9(11):1862–1875.
50. Jin SM, Youle RJ. The accumulation of misfolded proteins in the mitochondrial matrix is sensed by PINK1 to induce PARK2/Parkin-mediated mitophagy of polarized mitochondria. *Autophagy*. 2013;9(11):1750–1757.
51. Joselin AP, et al. ROS-dependent regulation of Parkin and DJ-1 localization during oxidative stress in neurons. *Hum Mol Genet*. 2012;21(22):4888–4903.
52. Hara H, et al. Mitochondrial fragmentation in cigarette smoke-induced bronchial epithelial cell senescence. *Am J Physiol Lung Cell Mol Physiol*. 2013;305(10):L737–L746.
53. Rabinovich RA, et al. Mitochondrial dysfunction in COPD patients with low body mass index. *Eur Respir J*. 2007;29(4):643–650.
54. Puente-Maestu L, et al. Abnormal mitochondrial function in locomotor and respiratory muscles of COPD patients. *Eur Respir J*. 2009; 33(5):1045–1052.
55. Bonapace L, et al. Induction of autophagy-dependent necroptosis is required for childhood acute lymphoblastic leukemia cells to overcome glucocorticoid resistance. *J Clin Invest*. 2010;120(4):1310–1323.
56. Bell BD, et al. FADD and caspase-8 control the outcome of autophagic signaling in proliferating T cells. *Proc Natl Acad Sci U S A*. 2008;105(43):16677–16682.
57. Khan MJ, et al. Inhibition of autophagy rescues palmitic acid-induced necroptosis of endothelial cells. *J Biol Chem*. 2012;287(25):21110–21120.
58. Gomes LC, Benedetto GD, Scorrano L. During autophagy mitochondria elongate, are spared from degradation and sustain cell viability. *Nat Cell Biol*. 2011;13(5):589–598.
59. Wang Z, Jiang H, Chen S, Du F, Wang X. The mitochondrial phosphatase PGAM5 functions at the convergence point of multiple necrotic death pathways. *Cell*. 2012;148(1–2):228–243.
60. Zhang DW, et al. RIP3, an energy metabolism regulator that switches TNF-induced cell death from apoptosis to necrosis. *Science*. 2009;325(5938):332–336.
61. Tait SWG, et al. Widespread mitochondrial depletion via mitophagy does not compromise necroptosis. *Cell Rep*. 2012;5(4):878–885.
62. Scarffe LA, Stevens DA, Dawson VL, Dawson TM. Parkin and PINK1: much more than mitophagy. *Trends Neurosci*. 2014;37(6):315–324.
63. Wirawan E, et al. Beclin1: a role in membrane dynamics beyond. Autophagy. 2012;8(1):6–17.
64. Subramani S, Malhotra V. Non-autophagic roles of autophagy-related proteins. *EMBO Rep*. 2013;14(2):143–151.
65. Fu M, St-Pierre P, Shankar J, Wang PT, Joshi B, Nabi IR. Regulation of mitophagy by the Gp78 E3 ubiquitin ligase. *Mol Biol Cell*. 2013;24(8):1153–1162.
66. Chen BB, et al. E3 ligase subunit Fbxo15 PINK1 kinase regulate cardiolipin synthase 1 stability mitochondrial function in pneumonia. *Cell Rep*. 2014;7(2):476–487.
67. Kitada, T, et al. Impaired dopamine release and synaptic plasticity in the striatum of PINK1-deficient mice. *Proc Natl Acad Sci U S A*. 2007;104(27):11441–11446.
68. Goldberg MS, et al. Parkin-deficient mice exhibit nigrostriatal deficits but not loss of dopaminergic neurons. *J Biol Chem*. 2003;278(44):43628–43635.
69. Gautier CA, Kitada T, Shen J. Loss of PINK1 causes mitochondrial functional defects increased sensitivity to oxidative stress. *Proc Natl Acad Sci U S A*. 2008;105(32):11364–11369.
70. An CH, et al. TLR4 deficiency promotes autophagy during cigarette smoke-induced pulmonary emphysema. *Am J Physiol Lung Cell Mol Physiol*. 2012;303(9):L748–L757.
71. Kim HP, Chen ZH, Choi AM, Ryter SW. Analyzing autophagy in clinical tissues of lung and vascular diseases. *Meth Enzymol*. 2009;453:197–216.
72. Pauwels RA, et al. Global strategy for the diagnosis, management, and prevention of chronic obstructive pulmonary disease. NHLBI/WHO Global Initiative for Chronic Obstructive Lung Disease (GOLD) Workshop summary. *Am J Respir Crit Care Med*.2001;163(5):1256–1276.